공학석사 학위논문

Flow-field/electrode unified membrane-electrode assemblies using graphene foam in polymer electrolyte membrane fuel cells

그래핀 폼을 이용한 유로/전극 일체형
막-전극접합체 고분자전해질 연료전지

2016년 2월

서울대학교 대학원
공과대학 화학생물공학부 에너지환경화학융합기술전공
박지은

Abstract

Flow-field/electrode unified membrane-electrode assemblies using graphene foam in polymer electrolyte membrane fuel cells

Ji Eun Park

School of Chemical & Biological Engineering

Chemical Convergence for Energy & Environment

The Graduate School

Seoul National University

Fuel cells are electrochemical energy conversion devices that directly convert chemical energy to electrical energy. Among various kinds of fuel cells, polymer electrolyte membrane fuel cells (PEMFCs) are attractive for transportation and portable electronics due to low operating temperature, high power density, and short start-up time. However, high cost components, scarcity of catalyst, and poor durability have limited the commercialization. Therefore many reports have focused on two ways: one is to develop inexpensive and durable electro-catalyst by reducing the use of platinum or

replacing platinum with other nonprecious catalysts. The other is to enhance performance of single cell by improving structure of catalyst layer or modifying flow field of bipolar plate and gas diffusion layer.

Recent researches have shown substituting conventional flow field for porous metal materials such as metal powder, metal coil, metal mesh, and metal foam, which have novel structures, increased cell performance by improving mass transport of reactant and product. Furthermore, some reports eliminated gas diffusion layer (GDL) from membrane-electrode assembly (MEA) by using these materials as multifunctional materials of GDL and flow field. These design reduced reactant pathway from bipolar plate to catalyst layer, and mass transport resistance, resulting in increased performance of single cell.

This thesis focused on the enhancement of performance of PEMFCs by substituting graphene foam with cell components. Graphene foam is three-dimensional graphene-based material having advantage of graphene and structural characteristics of metal foam. Various kinds of the metal materials have drawbacks in PEMFCs operating condition. Metal is highly susceptible to corrosion in acidic condition and metal ion can contaminate MEA. Therefore, graphene foam is promising material that has novel structures without the use of metal.

The ultimate objective is to fabricate unified MEA by using graphene foam as GDL and flow field. Compressed graphene foam can play role in

GDL as well as flow field. This design reduces reactant pathway from bipolar plate to catalyst layer, mass transport resistance, and thickness of MEA, resulting in increased performance of single cell and volume power density of stacks. To prepare unified MEA, the effect of graphene foam on flow field and GDL were investigated. Firstly, cell test, oxygen gain, and electrochemical impedance spectroscopy (EIS) were conducted to examine of the effect of graphene foam as flow field to enhanced mass transport. These results have shown that graphene foam as flow field distributed uniformly reactants on entire area and removed generated water by inhibiting water flooding.

Secondly, single cell that integrated gas diffusion layer (GDL) with flow field was conducted to investigate the effect of unified MEA on cell performance. Eliminating GDL in MEA by using graphene foam as multifunctional material of GDL and flow field reduced electrical and mass transport resistance, and thickness of MEAs, leading to enhanced performance and increased volume power density. As a result, GDL-less MEA increased power density by 50% and decreased thickness of MEA by 90%, resulting in enhanced volume power density. Therefore, graphene foam can play role in GDL and flow field.

Keywords: Polymer electrolyte membrane fuel cells (PEMFCs), graphene foam, flow field, gas diffusion layer (GDL), unified membrane-electrode

assembly (MEA).

Student Number: 2014-20628

Contents

Abstract ..... **i**

Contents ..... **v**

List of Tables ..... **vii**

List of Figures ..... **viii**

Chapter 1. Introduction **1**

1.1 Polymer Electrolyte Membrane Fuel Cells 1

1.1.1 Principle 1

1.1.2 Cell Components 2

1.1.3 Challenges of PEMFC 11

1.2 Overpotentials of PEMFC 13

1.2.1 Activation Overpotential 13

1.2.2 Ohmic Overpotential 15

1.2.3 Concentration Overpotential 17

1.3 Ultimate Objective of This Dissertation 18

Chapter 2. Experimental **21**

2.1 Fabrication of graphene foam MEA which applied graphene foam on flow field of bipolar plates 21

2.2 Fabrication of graphene foam MEA which applied graphene foam on

GDL-less MEA…….…….23

2.3 Characterization of the graphene foam……...……...25

2.4 Electrochemical characterization of graphene foam MEAs……..25

Chapter 3. Results and Discussion.....27

3.1 Application of graphene foam on flow-field of bipolar plates in polymer electrolyte membrane fuel cells……...27

3.2 Application of graphene foam on gas diffusion layer–less membrane-electrode assembly in polymer electrolyte membrane fuel cell…….44

Chapter 4 Conclusions 65

References…….....67

Korean Abstract.....75

List of Tables

Table 3.1 Porosity of graphene foams (%).....28

Table 3.2 Comparison in current density of each MEA.....33

Table 3.3 Comparison in current density of 200um-GF MEA and conventional MEA.....54

List of Figures

Figure 1.1 Schematic representation of PEMFCs single cell. Taken from reference [3] 3

Figure 1.2 Polymer Electrolyte Membrane Fuel Cells Cell Components….....4

Figure 1.3 Chemical structure of Nafion, membrane used in PEMFCs. Taken from reference [5].....6

Figure 1.4 Schematic of the catalyst layer in PEMFCs. Taken from reference [6] 7

Figure 1.5 Schematic of fuel cell I-V curve. Taken from reference [22].....14

Figure 1.6 Effect of exchange current density (j_0) on cell performance. Taken from reference [2].....16

Figure 2.1 (a) Schematic of PEMFC with graphene foam as flow field and conventional flow field, and (b) Photograph of bipolar plates used for this study. 22

Figure 2.2 Schematic of conventional MEA and graphene foam MEA which applied graphene foam on GDL-less MEA. 24

Figure 3.1 SEM images of graphene foams (a) top view and (b) cross-sectional view of graphene foam before compression, and (c) top view and (d) cross-sectional view of graphene foam after compression.....29

Figure 3.2 Polarization curves of graphene foam MEAs. (a) Polarization curves of uncompressed graphene foam MEA and conventional MEA, and (b) Polarization curves of compressed graphene foam MEA and conventional MEA. For both MEAs, the catalyst loading was 0.2 $mg \cdot cm^{-2}$. Test at 70 °C, a fully humidified H_2/air. 30

Figure 3.3 Polarization curves and difference between power densities with total outlet pressure of 180 kPa (a) Polarization curves of compressed graphene foam MEA and conventional MEAs, and (b) Difference between the power densities of compressed graphene foam MEA and conventional MEA. For both MEAs, the catalyst loading was 0.2 $mg \cdot cm^{-2}$. Test at 70 °C H_2/air, fully humidified with total outlet pressure of 180 kPa.....32

Figure 3.4 Oxygen gain graph with compressed graphene foam MEA and conventional MEA.....35

Figure 3.5 Electrochemical impedance spectroscopy (a) Randles equivalent circuit model for EIS. EIS Nyquist plots of compressed graphene foam MEA and conventional MEA at (b) 0.8 and (c) 0.4 V under a fully humidified H2/air with total outlet of 180 kPa 36

Figure 3.6 Schematic representation of reactant flow in flow field of (a) compressed graphene foam MEA and (b) conventional MEA.....39

Figure 3.7 Contact angles of water droplets on (a) graphene foam and (b) conventional flow field…….....40

Figure 3.8 Schematic representation of water removal of (a) compressed graphene foam MEA and (b) conventional MEA.....43

Figure 3.9 (a) Schematic of MEAs with flow field and without flow field. (b) Polarization curve of MEAs with flow field and without flow field. Test at 70 °C H2/O2, fully humidified with ambient pressure.....46

Figure 3.10 SEM images of graphene foams (a) top view of pristine graphene foam, and cross-sectional view of (b) pristine graphene foam, (c) 250 μm, (d) 200 μm, (e) 150 μm, and (f) 100 μm.....48

Figure 3.11 Polarization curve of MEAs with varying graphene foam thicknesses.....50

Figure 3.12 Polarization curves 200 μm-GF MEA and conventional MEA with ambient pressure. For both MEAs, the catalyst loading was 0.2 mg·cm-2. Test at 70 °C H2/air with ambient pressure.....53

Figure 3.13 Oxygen gain graph with 200 μm-GF MEA and conventional MEA in high current densities.....56

Figure 3.14 Electrochemical impedance spectroscopy (a) Randles equivalent circuit model for EIS. EIS Nyquist plots of 200 μm-GF MEA and conventional MEA at (b) 0.4 and (c) 0.8 V under a fully humidified H2/air.....58

Figure 3.15 (a) Schematic of 200 μm-GF MEA and 200 μm-GF MEA with GDL. (b) Polarization curve of 200 μm-GF MEA and 200 μm-GF MEA with GDL. (c) IR-corrected voltage of 200 μm-GF MEA and 200 μm-GF MEA

with GDL. Test at 70 °C H2/air, fully humidified with ambient pressure.....61

Figure 3.16 Electrochemical impedance spectroscopy of 200 μm-GF MEA and 200 μm-GF MEA with GDL at 0.6 V.....62

Chapter 1. General Introduction

1.1 Polymer Electrolyte Membrane Fuel Cells (PEMFCs)

1.1.1 Principle

Fuel cells are electrochemical energy conversion devices that directly convert chemical energy to electrical energy. Hydrogen fuel cell is the most common. In hydrogen fuel cell, two electrochemical reaction occurs in two electrodes, respectively. Anode reaction is hydrogen oxidation reaction and cathode reaction is oxygen reduction reaction.

Anode :	$H_2 \rightarrow 2H^+ + 2e^-$	E^0=0.000V
Cathode :	$½\ O_2 + 2H^+ + 2e^- \rightarrow H_2O$	E^0=1.229V
Overall :	$H_2 + ½\ O_2 \rightarrow H_2O$	E^0=1.229V

Various kinds of fuel cells have been developed according to the electrolyte. Among these fuel cells, polymer electrolyte membrane fuel cells (PEMFCs) are attractive for transportation and portable electronics due to low operating temperature, high power density, and short start-up time. PEMFCs are fuel cell using a membrane electrolyte, which is based on a polymer backbone with side-chains possessing acid-based groups [1]. The

most commonly used membrane is Nafion (Dupont). Protons produced in anode flow from anode to cathode through membrane and react with oxygen in cathode. Electrons generated by two electrochemical half reactions flow through an external circuit, constituting an electric current. To produce electricity, the major steps take place in fuel cell.

1. Reactant transport into the fuel cell
2. Electrochemical reaction
3. Ionic conduction through the electrolyte and electron conduction through the external circuit
4. Product removal from the fuel cell. [2]

1.1.2 Cell Components

Single cell of PEMFCs consists of membrane, catalyst layer, gas diffusion layer (GDL), and bipolar plates. Figure 1.2 shows that the componetns and structure of PEMFCs single cell.

Membrane

Membrane is thin electrolyte that conducts protons from anode to cathode. It transports the protons, which is generated in anode reaction from anode to cathode. Also, it is seperator beween anode and cathode to react the two electrochemical half reactions. Additionally, it is electronic insulator to

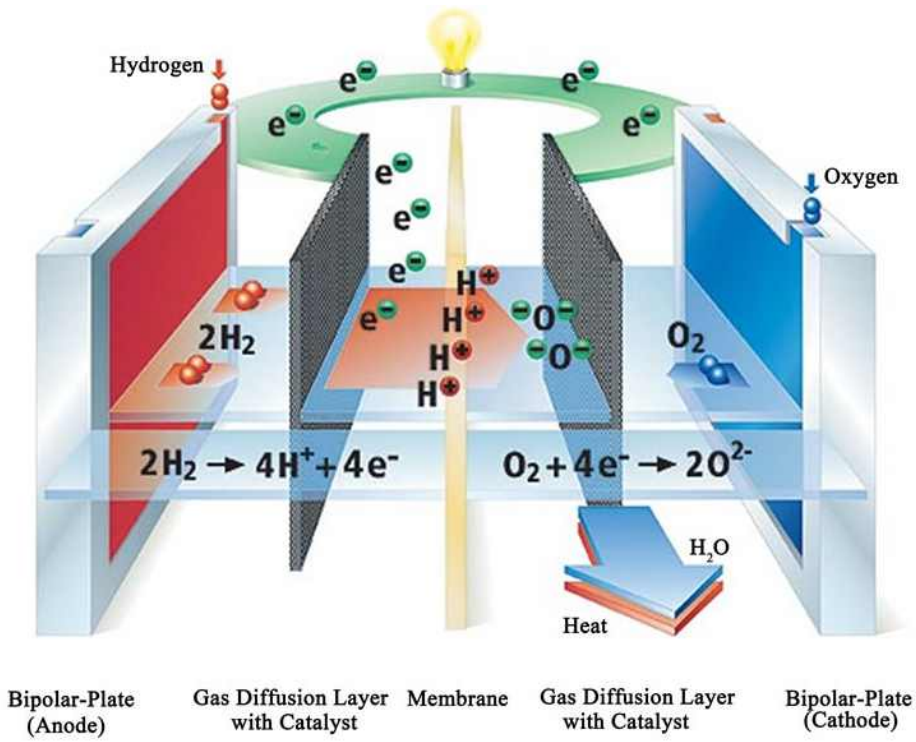

Figure 1.1 Schematic representation of PEMFCs single cell. Taken from reference [3]

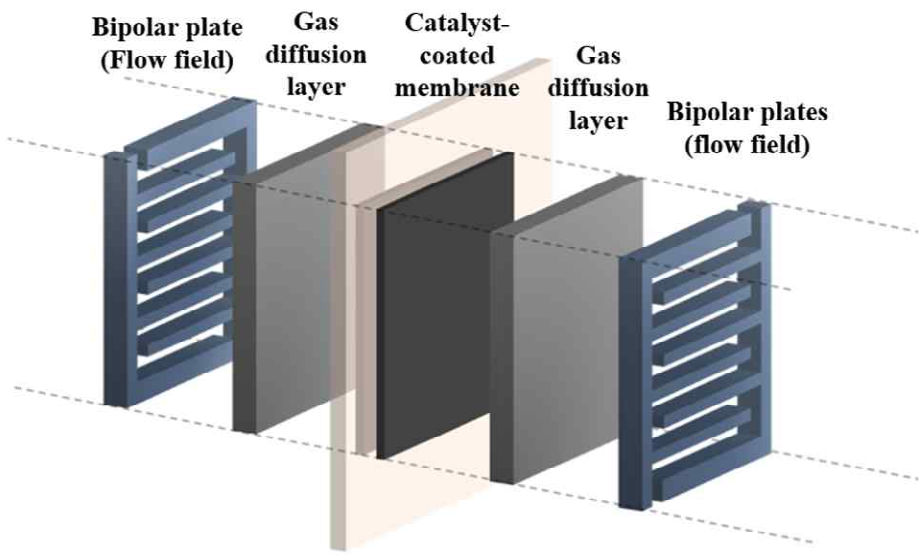

Figure 1.2 Polymer Electrolyte Membrane Fuel Cells Cell Components

prevent electron tranport. [1, 2] The most commonly used polymer electrolyte membrane is Nafion (Dupont), which has a backbone structure of polytetrafluoroethylene (PTFE) and sulfonic acid functional groups (Figure 1.3). These sulfonic acid functional groups are sites that transport protons. Two major transport occur in Nafion: one is vehicular diffusion, and the other if hopping mechanism. Vehicular diffusion is that protons transport from anode to cathode by forming hydronium ions combined water and protons. Hopping mechanism is that protons move directly from one site to another when sulfonic groups are connected due to sufficient water in Nafion [4].

Catalyst layer

Catalyst layer is where electrochemical reaction such as hydrogen oxidation reactant in anode, and oxygen reduction reaction in cathode occurs. Catalyst layer consists of catalyst, ionomer, and void space [1]. Electrochemical reaction ocuurs in three-plase boundaries, which consist of protons, electrons, and gases, as shown Figure 1.4. Therefore, transport of protons, electrons, and gases is vital for electrochemical reaction. First, protons transport from membrane to the catalyst through nafion ionomer. As interface between the membrane and catalyst is critical, two catalyst layers (anode and cathode) are fabricated directly in membrane, which is called catalyst-coated

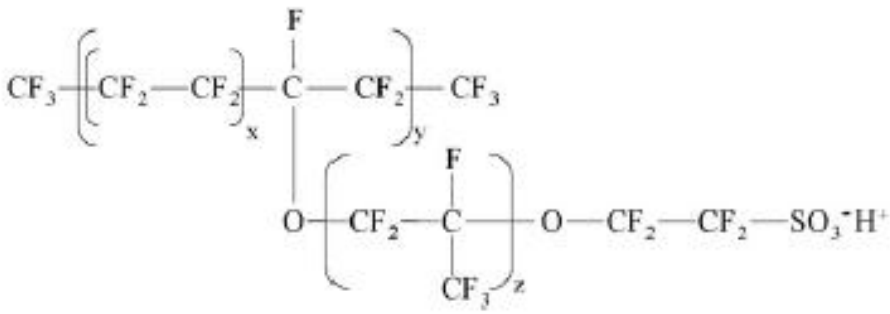

Figure 1.3 Chemical structure of Nafion, membrane used in PEMFCs. Taken from reference [5]

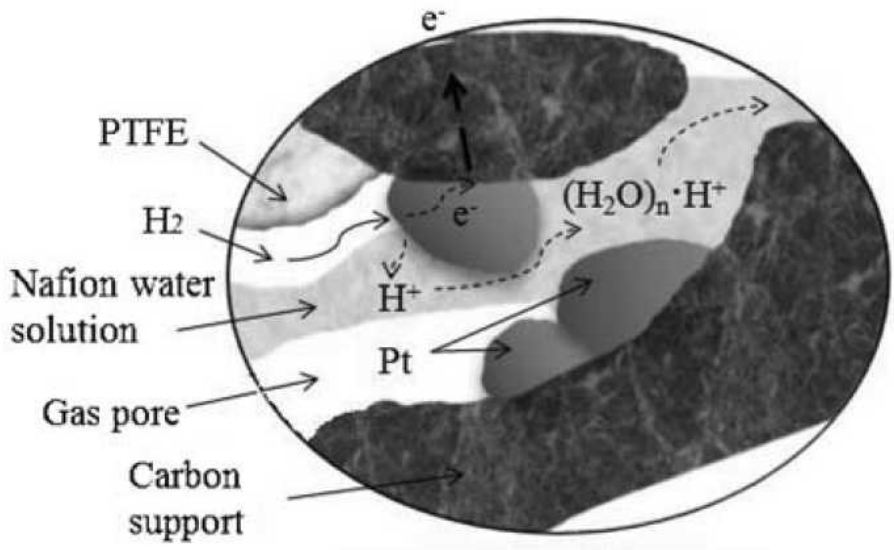

Figure 1.4 Schematic of the catalyst layer in PEMFCs. Taken from reference [6]

membrane (CCM). Secondly, electrons transport from the bipolar plate to the catalyst layer through gas diffusion layer. Finally, the reactant gases and product transport to and from the catalyst layer and flow field [7]. Therefore, catalyst layer must consist of interconnected pores for transport.

Gas diffusion layer (GDL)

Gas diffusion layer (GDL) is porous carbon material made by pressing carbon fibers into a carbon paper. It diffuses reactants from channel of bipolar plates to catalyst layer and removes generated water outside of catalyst layer. Additionally, it connects electron transport between bipolar plates and catalyst layer, and provides mechanical support to MEA [1]. GDL is important component for mass transport of fuel cell [8]. High porosity (~80%) of GDL can transport reactant into catalyst layer in through-plane direction. Among many kinds of GDLs, conventional GDL consists of polytetrafluoroethylene (PTFE)-treated carbon paper and micro-porous layer (MPL). PTFE coating, which is hydrophobic treatment, helps remove water from catalyst layer and prevent water flooding. MPL acts as smooth layer that provides large surface area for catalyst and good contact between porous carbon paper and catalyst layer. Recently, various kinds of metal foams as promising alternative [9, 10] have been applied on gas diffusion layer of PEMFCs to provide higher electronic conductivity and more directional

porous channel of reactants and product.

Bipolar plate (flow field)

Bipolar plates are important components of fuel cell for mass transport, which are on the outside of the membrane-electrode assemblies (MEAs). Functions of bipolar plates are passage for reactant and product, electrical connection, and mechanical support to the MEAs. Bipolar plates require flow field to distribute reactants, remove water, manage heat, and connect electrons [11]. In PEMFCs which is low temperature fuel cell (~80 °C), water removal capability is crucial for flow field design because water flooding in channel blocks gas transport and decreases cell performance. Therefore, two approaches have been developed to enhance mass transport of reactant and water removal: one is modifying channel/rib distribution of conventional flow field, and the other is using new materials having novel structures. Firstly, parallel, serpentine, and integrated type flow field are developed by modifying the channel-rib distribution [11, 12]. In channel/rib flow field, channel provides reactant and product transport, and rib connects electrons to GDL. Various kinds of channel/rib flow field have been developed to improve distribution of reactants and inhibit water flooding by removing generated water in channel of flow field. Among these flow fields, conventional flow field is serpentine flow field, which has long reactant

pathway. Serpentine flow field can distribute reactant uniformly, and help removal of water in vapor form. [11]. However, rib of flow field causes to block reactant transport and accumulate water, hindering water removal [13, 14]. Water flooding declines performance at high current density. Also, gas diffusion layer under ribs is compressed during cell assembly. This region decreased porosity and mass transport.

Additionally, new types of flow field such as porous metallic powder [14-16], micro-coil [17], and metal foam [18-21] are introduced in bipolar plates to improve mass transport of reactants and products. These structures are open structures to distribute reactants on entire area and remove generated water by inhibiting water flooding.

1.1.3 Challenges of PEMFCs

Polymer electrolyte membrane fuel cells (PEMFCs) are attractive for transportation and portable electronics due to low operating temperature, high power density, and short start-up time. However, high cost components, scarcity of catalyst, and poor durability have limited the commercialization. Therefore many reports have focused on two ways: one is to develop inexpensive and durable electro-catalyst by reducing the use of platinum or replacing platinum with other nonprecious catalysts. The other is to enhance performance of single cell by improving structure of catalyst layer or modifying flow field of bipolar plate and gas diffusion layer.

Commercially used catalyst is platinum supported carbon (Pt/C), which exhibited the highest catalytic activity. However, many researches such as Pt-Metal alloy [22, 23], core-shell [24] and hollow catalyst [25] have been developed for total platinum loading reduction as platinum is expensive and scarce. Non-metal catalysts such as b, n, s-doped and co-doped carbon-based materials also have been reported. Therefore, inexpensive and durable non-novel catalysts seem to be developed for commercialization.

Additionally, fuel cell components such as flow field, GDL, and catalyst layer have been modified to enhance performance of single cell. Flow field is important for distributing reactants and removing water. Modifying design of flow field [11, 12] or substituting new porous materials [18-21] on flow

field enhanced mass transport by inhibiting water accumulation. Also, structures of catalyst layer have been modified to provide highly porous structure for improved mass transport [26]. This macro-porous inverse-opal structure had interconnected pores and provided high porosity in catalyst layer, resulting in enhancement of performance. Thus new approach of modifying MEA structure is needed to decrease mass transport loss and increase the cell performance.

1.2 Overpotentials of PEMFCs

Although equilibrium voltage (E_0) of PEMFCs is 1.229 V, actual voltage (E) of PEMFCs reduces from equilibrium cell voltage due to three losses. as shown in Figure 1.5 [27]. Three losses are activation, ohmic, and concentration (mass transport) overpotential. Activation loss ($\eta_{act)}$ is related to reaction kinetics of catalyst. Ohmic loss (η_{ohmic}) is due to resistance to ionic and electron transport. Concentration loss ($\eta_{conc)}$ arises from reactant transport resistance to the active sites of catalyst layer [28].

$$E = E_0 - \eta_{act} - \eta_{ohmic} - \eta_{conc}$$

1.2.1 Activation Overpotential

Activation overpotential depends on low catalytic activity, and sluggish reaction kinetics [29]. Activation overpotential is associated with the reaction kinetic parameters and occurs at low current densities.

$$\eta_{act} = a + b \log j \text{ [28]}$$

where $a = RT\ln j_0/\alpha nF$, and $b = RT/\alpha nF$.

It is known as the Tafel equation, simplified Butler-Volmer equation. Exchange current density (j_0) is current density at equilibrium when the net reaction rate is zero and indication of the rate of reaction at equilibrium.

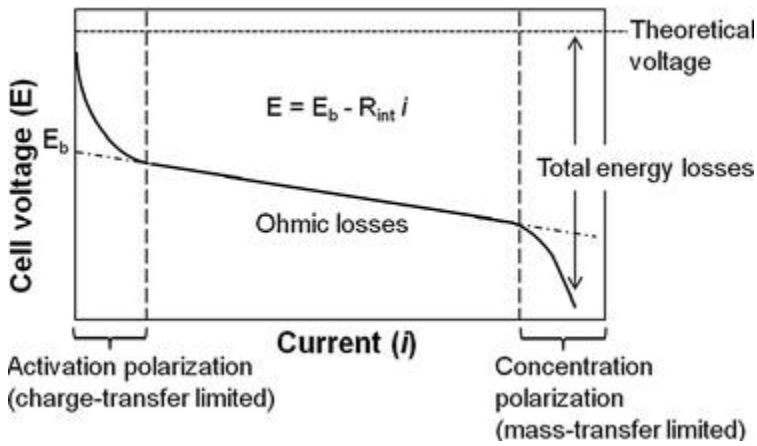

Figure 1.5 Schematic of fuel cell I-V curve. Taken from reference [27]

$$j_0 = nFC_R f_1 e^{-\Delta G1/(RT)} \quad [2]$$

where n is the number of electrons in electrochemical reaction, c_R is actual concentrations of reactants, f_1 is decay rate to products, ΔG_1 is the activation barrier for the reaction, and T is temperature.

As shown in Figure 1.6, high j_0 means low activation loss, leading to high performance. To reduce activation loss, it is needed to increase temperature, use more effective catalyst by decreasing activation barrier, increase reactant concentration by higher pressure, or increase the number of possible sites [2].

1.2.2 Ohmic Overpotential

Ohmic overpotential is loss due to ionic and electronic conductivity and dominant in middle current densities.

$$\eta_{ohmic} = iR_{ohmic}$$

R_{ohmic} is cell internal resistance, consisting of ionic resistance of the membrane, electrical resistance of GDL, and all contact resistances [29]. Ohmic loss can be reduced to use highly ion-conductive membrane and highly electron-conductive GDL, and decrease contact resistances.

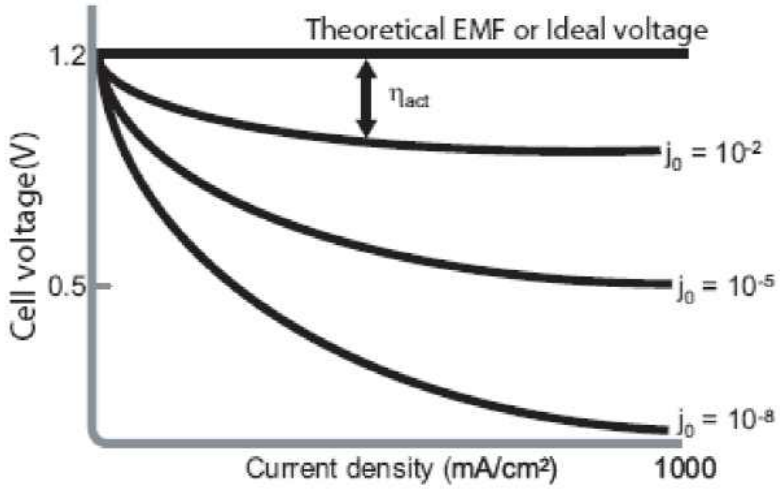

Figure 1.6 Effect of exchange current density (j_0) on cell performance. Taken from reference [2]

1.2.3 Concentration Overpotential

Concentration overpotential is related to mass transport resistances of reactants and product. Reactants must be transported from bipolar plates to catalyst layer through GDL. Also generated water must be transported from catalyst layer to bipolar plates to inhibit water flooding.

$$\eta_{conc} = c \ln j_L/(j_L-j) \quad [2]$$

where c is $RT/\alpha nF$, j_L is limiting current density.

$$j_L = nFD_{eff}C_R/\delta$$

where D_{eff} is effective reactant diffusivity in catalyst layer, C_R is reactant concentration, and δ is electrode thickness.

To reduce concentration loss, j_L must be increased. First, modifying flow field in bipolar plates increased C_R by distributing reactant and remove water. Also electrode structure and electrode thickness are optimized to increase $D_{eff,}$ and decrease δ [2]. Additionally, mass transport limitations are also due to diffusional resistances across the GDL [30].

1.3 Ultimate Objective of This Dissertation

Actual voltage of PEMFCs reduces from equilibrium cell voltage due to three losses. Three losses are activation, ohmic, and concentration (mass transport) overpotential. Minimizing these losses leads to enhancing performance of PEMFCs. Among these losses, mass transport overpotential can be reduced by enhancing mass transport of reactant and water removal in flow field of bipolar plates.

Recent researches have shown substituting conventional flow field for porous metal materials such as porous metallic powder [14-16], micro-coil [17], and metal foam [18-21], which have novel structures, increased cell performance by improving mass transport of reactant and product. These structures are open structures by eliminating the drawbacks of rib in conventional flow field. Among these new materials, many studies [18-21] have been reported that metal foam as flow field improved mass transport and enhanced performance of single cell. Reddy et al [18] proposed metal foam as flow field of bipolar plates in PEMFC. Compared with conventional flow field, lower through-plane permeability of metal foam caused tortuous reactant pathway, leading to flow of gases based on convection as well as diffusion. Wang [19] applied various metal foam on flow field in low humidity operation to evaluate the effect of high thermal and electrical conductivity of metal foam on performance. They found that application of

metal foam on flow field enhanced heat management and electron transport because solid phase is more conductive than gas phase. Tseng et al [21] replaced conventional flow field with polytetrafluoroethylene (PTFE)-treated nickel foam. High porosity of nickel foam provided uniform distribution of reactants and hydrophobicity of PTFE-treated nickel foam inhibited water flooding, resulting in enhanced performance when using oxygen. However, these metal foams are highly susceptible to corrosion in polymer electrolyte membrane fuel cell operation condition. Also, MEAs are contaminated with metal ion because of the use of metal components.

Cheng el al [31] reported graphene foam (GF) as three-dimensional graphene-based material. Graphene foam is free-standing foam prepared by deposition of graphene on nickel foams, followed by etching nickel foams. This material is a promising candidate for flow field because it integrates structural advantage of metal foams with graphene. It can also improve the drawbacks of metal foam as flow field by using graphene instead of metal.

Furthermore, some reports eliminated gas diffusion layer (GDL) from membrane-electrode assembly (MEA) [17, 32] by using metal materials and micro-porous layer (MPL) as GDL and flow field. These design substituted GDL with MPL and metal components. By decreasing thickness of electrodes, mass transport loss was decreased.

In this thesis, flow-field/electrode unified membrane-electrode assemblies (MEA) are proposed to integrate GDL and flow field using graphene foam. Flow field is important to in-plane reactant transport and GDL is critical to through-plane reactant transport. As graphene foam has interconnected in-plane and through-plane pores, graphene foam is appropriate for multifunctional component of GDL and flow field. Unlike other researches [16, 17, 21, 32], graphene foam is applied on MEA without treatment and MPL. To fabricate unified MEA, it is needed to investigate the effect of graphene foam on flow field and GDL, respectively. Firstly single cell test, oxygen gain, and electrochemical impedance spectroscopy were evaluated to investigate the influence of graphene foam as flow field on the improved mass transport of reactants and water removal. Secondly, graphene foam was applied on GDL-less MEA without any treatment and MPL. As the thickness of MEA was decreased by 85%, mass transport resistance was reduced by decreased reactant pathway and volume power density was also increased.

Chapter 2. Experimental

2.1 Fabrication of graphene foam MEA which applied graphene foam on flow field of bipolar plates

Membrane electrode assembly (MEA) fabrication procedure has been reported [26, 33]. MEA were fabricated using the catalyst coated membrane (CCM) type. The polymer electrolyte membrane was Nafion 212 that was treated with 2.5% hydrogen peroxide at 80 °C for 1h, then rinsed boiling deionized water for 1h. The membrane was immersed in 0.5 M sulfonic acid at 80 °C for 1h, and rinsed deionized water at 80 °C for protonation. The anode and cathode catalyst layer were 0.2 $mg \cdot cm^{-2}$ 40 wt% Pt/C (Johnson Matthey Co.). Gas diffusion layer (GDL) (Sigracet 35BC, SGL group) was placed on both sides of the CCM.

Figure 2.1 (a) shows the schematic diagram of PEMFCs with graphene foam as flow field (graphene foam MEA) and conventional flow field (conventional MEA). The graphene foam with pores of 580um and thickness of 1mm was obtained from Graphene Supermarket, Inc.. Compared with conventional MEA in which inserted into single cell which had single serpentine type flow field in bipolar plates, the graphene foam was placed in bipolar plate as shown in Figure 2.1 (b). Then the gasket was placed around

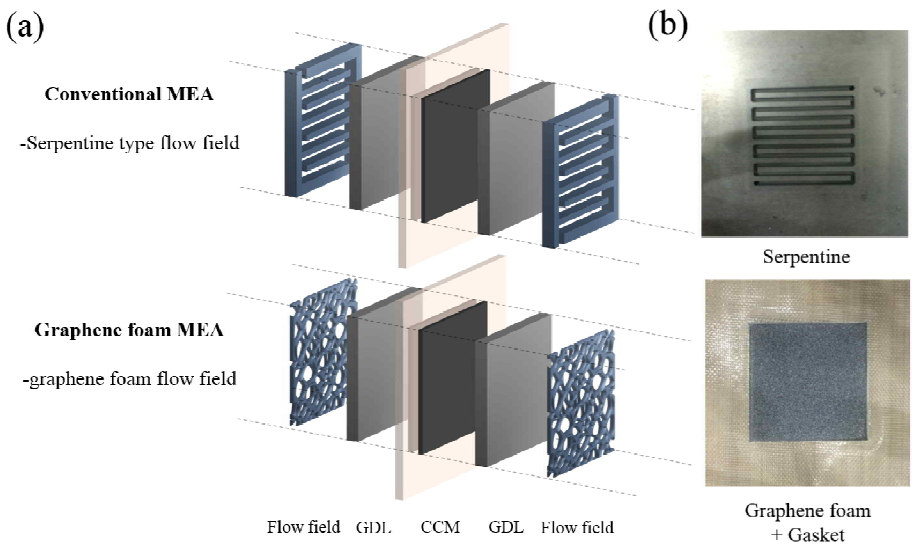

Figure 2.1 (a) Schematic of PEMFC with graphene foam as flow field and conventional flow field, and (b) Photograph of bipolar plates used for this study.

graphene foam to seal gases and control easily the thickness of graphene foam. In this work, the graphene foam was compressed during cell assembly to enhance electrical conductivity [21] and diffuse more reactants into GDL by making tortuous in-plane pathway.

2.2 Fabrication of graphene foam MEA which applied graphene foam on GDL-less MEA

Figure 2.2 shows the schematic diagram of PEMFCs using graphene foam (Graphene Supermarket, Inc.) as combined components of GDL and flow field (GF MEA), and conventional PEMFCs (conventional MEA). Conventional MEA consists of catalyst coated membrane (CCM), GDL, and flow field in bipolar plates. On the other hand, graphene foam MEA includes catalyst coated membrane (CCM) and graphene foam, which serves as GDL and flow field. Graphene foam MEA do not have GDL by replacing GDL and conventional flow field with graphene foam. In other words, graphene foam MEA is GDL-less MEA and uses graphene foam as multi-functional component.

Graphene foam was compressed during cell assembly to diffuse more reactants into GDL and conductivity of graphene foam as described in 2.1. Decreased thickness of graphene foam made smaller in-plane pores of foam and increased reactants diffused into GDL. Also, thinner flow field induced

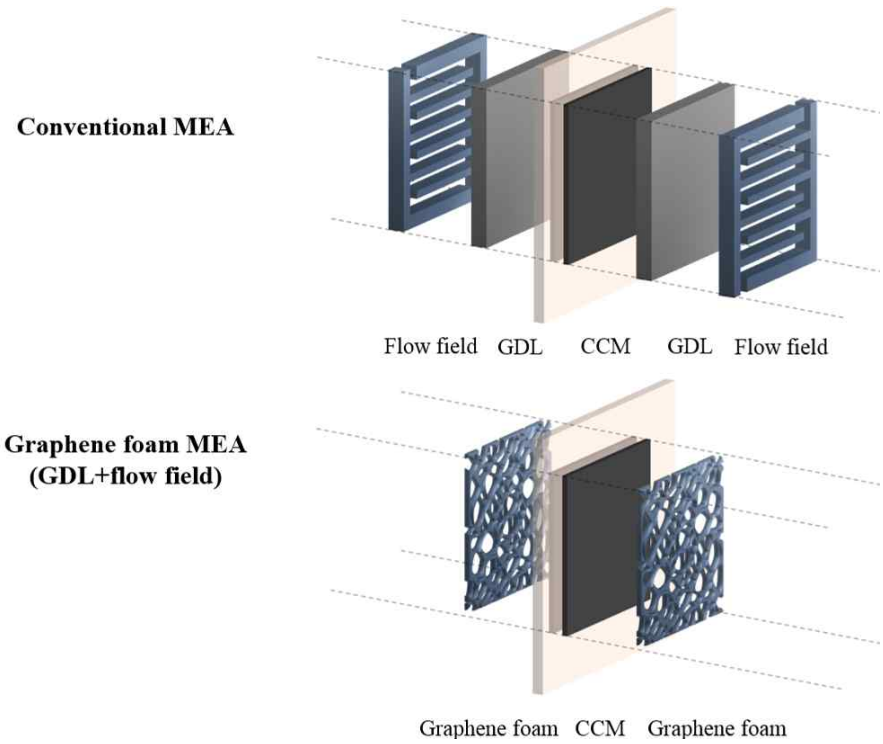

Figure 2.2 Schematic of conventional MEA and graphene foam MEA which applied graphene foam on GDL-less MEA.

faster flow velocity compared with conventional flow field, leading to pulling water droplet on graphene foam and removing accumulated water. However, too thin graphene foam could cause blocking the reactant pathway. Therefore, thickness of graphene foam is optimized to provide an appropriate trade-off between conductivity of graphene foam and mass transport of reactant and product. To investigate this effect, four different graphene foam were tested having different thicknesses; 1 mm, 250 μm, 200 μm, 150 μm, 100 μm. (1 mm-GF MEA, 250 μm -GF MEA, 200 μm-GF MEA, 150 μm-GF MEA, and 100 μm-GF MEA)

2.3 Characterization of the graphene foam

The pore morphology and thickness of the graphene foam were characterized using FE-SEM (Carl Zeiss SUPRA 55VP). Mercury intrusion porosimetry (AutoPore IV 9500) was carried out to measure the porosity of graphene foams before and after compression. Contact angle analyzer (Phoenix 300) was conducted to analyze hydrophobicity of graphene foam and nickel foam by observing contact angles of water on surface of foams. Larger contact angle means that surface of foams is more hydrophobic [34].

2.4 Electrochemical characterization of graphene foam MEAs

The single cell performance of each MEA was measured with the active area being 5 cm^2 to investigate the effect of graphene foam as combined component of GDL and flow field. The thicknesses of graphene foam were controlled by using four different gaskets which had different thickness. Each graphene foam MEA was inserted into bipolar plates that had four different gaskets and graphene foams, respectively. The test was conducted using fully humidified H_2/air. The cell temperature was 70 °C.

Electrochemical impedance spectroscopy (EIS) (IM-6, Zahner) was measured while hydrogen and air were fed into the anode and cathode sides, respectively. The cell voltage of the EIS measurement was 0.8 and 0.4 V with an amplitude of 5 mV to characterize ohmic resistance, charge transfer resistance and mass transfer resistance. The measured frequency range was 100 mHz to 100 kHz.

Chapter 3. Results and discussion

3.1 Enhanced mass transport of fuel cells using three-dimensional graphene foam as flow field

Graphene foam is three-dimensional graphene-based material which has interconnected pores and high porosity. Graphene foam was compressed during cell assembly to use as flow field. The porosity and SEM images of graphene foam before and after compression are shown in Table 3.1 and Figure 3.1. Before compression, the thickness and porosity of graphene foam was 1 mm and 96.25%. High porosity of foam > 90% makes reactants not diffuse into GDL but just pass through flow field. So the performance of uncompressed graphene foam MEA was very low compared with conventional MEA as shown in Figure 3.2 (a). Therefore, thickness of graphene foam was decreased from 1mm to 150um to reduce porosity and pore size. Then, Figure 3.2 (b) shows that the performance of compressed graphene foam MEA was higher than uncompressed graphene foam MEA and comparable with conventional MEA. After compression, the porosity of graphene foam was slightly reduced but retained high porosity and porous structure. Reduced porosity by compression makes smaller pore in in-plane direction and then tortuous reactant pathway [21] thereby diffusing more

Table 3.1 Porosity of graphene foams (%)

	Pristine foam	Compressed foam
Porosity (%)	96.25	88.99

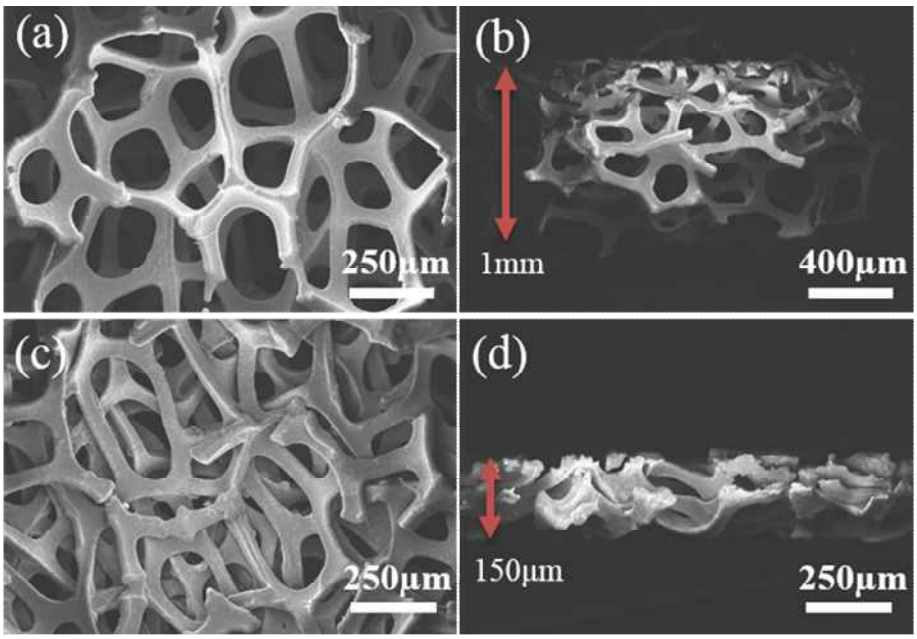

Figure 3.1 SEM images of graphene foams (a) top view and (b) cross-sectional view of graphene foam before compression, and (c) top view and (d) cross-sectional view of graphene foam after compression

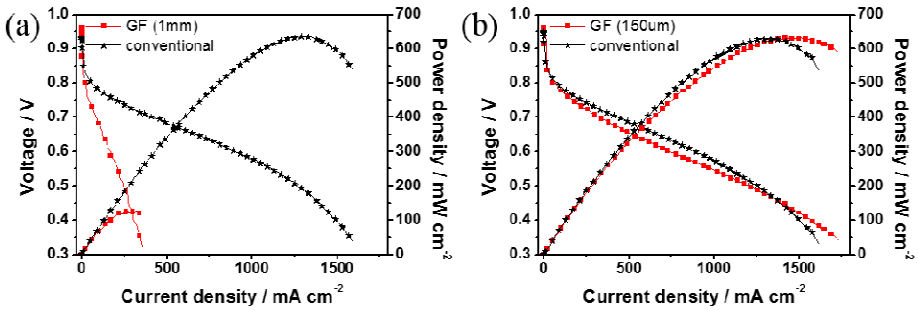

Figure 3.2 Polarization curves of graphene foam MEAs (a) Polarization curves of uncompressed graphene foam MEA and conventional MEA, and (b) Polarization curves of compressed graphene foam MEA and conventional MEA. For both MEAs, the catalyst loading was 0.2 mg·cm^{-2}. Test at 70 °C, a fully humidified H_2/air.

reactants into GDL.

Figure 3.3 (a) presents the polarization curves of compressed graphene foam MEA and conventional MEA. They were measured with a fully humidified hydrogen and air at 70 °C under total outlet pressure of 180 kPa. In high voltage region > 0.6 V, the performance of compressed graphene foam MEA is slightly lower than conventional MEA. This indicates that the conductivity of graphene foam is lower than conventional flow field since rib area is much smaller than channel area. Kuran et al [35] stated that thinner rid width and lower channel-rib ratio limit electron transport and reduce conductivity. However, the compressed graphene foam MEA showed higher current densities than conventional MEA in low voltage region < 0.6 V. For conventional MEA, cell voltage dropped as current density exceeds 1.5 $A \cdot cm^{-2}$. It is attributed to water flooding in cathode. On the other hand, the current density of compressed graphene foam MEA at 0.4 V was 2436 $mA \cdot cm^{-2}$, which is approximately 30% higher than conventional MEA as shown in Table 3.2. Also, Figure 3.3 (b) showed the difference between the power densities of two MEAs was 2436 $mA \cdot cm^{-2}$, which is approximately 30% higher than conventional MEA as shown in Table 3.2. Also, Figure 3.3 (b) showed the difference between the power densities of two MEAs was considerable in high current densities, which is dominant on concentration polarization related to mass transport. This suggests that graphene foam as

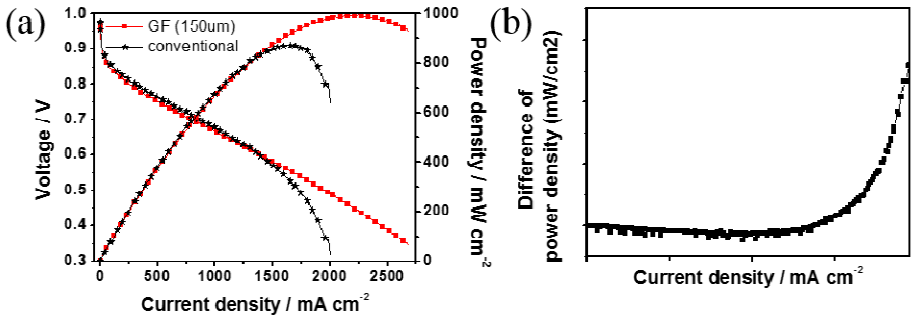

Figure 3.3 Polarization curves and difference between power densities with total outlet pressure of 180 kPa (a) Polarization curves of compressed graphene foam MEA and conventional MEAs, and (b) Difference between the power densities of compressed graphene foam MEA and conventional MEA. For both MEAs, the catalyst loading was 0.2 mg·cm^{-2}. Test at 70 °C H_2/air, fully humidified with total outlet pressure of 180 kPa.

Table 3.2 Comparison in current density of each MEA

	0.7 V	0.6 V	0.4 V
Graphene foam, 1.8bar ($mA \cdot cm^{-2}$)	798 (92%)	1397 (101%)	2436 (128%)
Conventional MEA, 1.8bar ($mA \cdot cm^{-2}$)	872	1383	1900

flow field reduced concentration loss by distributing reactants and removing generated water without flooding.

To concretely investigate the effect of graphene foam on enhanced mass transport, oxygen gain and electrochemical impedance spectroscopy were conducted. Oxygen gain experiment is measuring the difference in cell potential at given current density under oxygen-rich (O_2) condition and oxygen-depleted condition (air) [36]. In oxygen-rich condition, the mass transport resistance can be negligible. But cathode suffer from oxygen transport due to reduced oxygen partial pressure and blanketing effect of nitrogen in air condition [37]. By comparing the difference between cell voltage under oxygen and air condition, we can estimate mass transport resistance of MEA. Therefore, decreased oxygen gain indicates lower mass transport resistance, leading to enhanced mass transport. Figure 3.4 represents that oxygen gain of compressed graphene foam MEA is lower than that of conventional MEA in overall current densities region. The electrochemical impedance spectroscopy (EIS) results at 0.8 V and 0.4 V are shown in Figure 3.5. Figure 3.5 (a) represents the equivalent circuit of modified Randles model chosen for this study. R_Ω, R_{ct}, and Z_w indicate ohmic resistance, charge transfer resistance, and Warburg impedance, related to mass transport resistance. Figure 3.5 (b) and (c) are Nyquist plot, which is the plot of imaginary part of impedance versus the real part at each

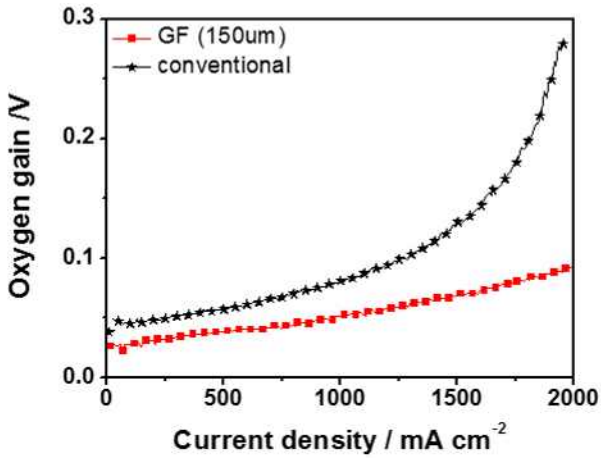

Figure 3.4 Oxygen gain graph with compressed graphene foam MEA and conventional MEA

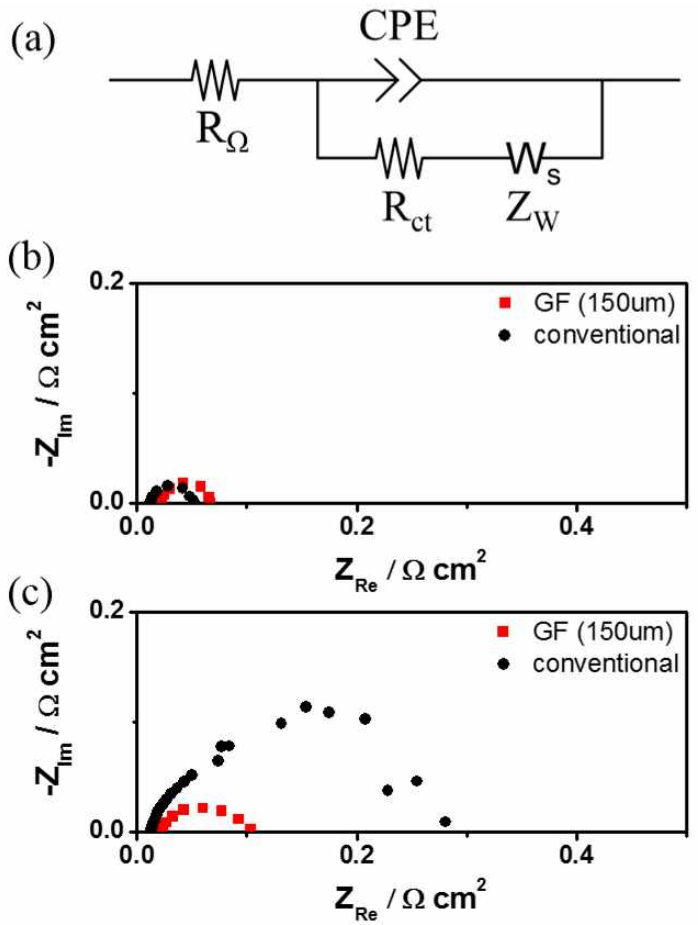

Figure 3.5 Electrochemical impedance spectroscopy (a) Randles equivalent circuit model for EIS. EIS Nyquist plots of compressed graphene foam MEA and conventional MEA at (b) 0.8 and (c) 0.4 V under a fully humidified H_2/air with total outlet of 180 kPa.

frequency. High-frequency intercept is ohmic resistance, R_{Ω}, which is the sum of the ionic and electronic resistances of cell components. The diameter of semicircle at high cell voltage (0.8 V) represents charge transfer resistance, R_{ct}. However, at low cell voltage (0.4 V), two arcs which indicate charge transfer (high frequency) and mass transport (low frequency) mixed together [38-41]. In Figure 3.5 (b), the Nyquist plot at 0.8 V shows single semicircle because activation kinetics is dominant and mass transport effect is neglected in high cell voltage. The ohmic and charge transfer resistance of compressed graphene foam MEA was slightly larger than that of conventional MEA because the electrical conductivity of graphene foam was lower than graphite due to low channel-rib ratio [35]. This was consistent result with polarization test in Figure 3.3 (a). However, the diameter of semicircle of compressed graphene foam MEA at 0.4 V was much smaller than that of conventional MEA as shown in Figure 3.5 (c) although the charge transfer resistance of compressed graphene foam MEA at 0.8 V was larger. The semicircle at 0.4 V includes two semicircle; charge transfer resistance (high frequency) and mass transport resistance (low frequency). Smaller diameter of this semicircle means lower mass transport resistance of graphene foam MEA. Thus this result indicates that application of graphene foam on flow field lowered mass transport resistance despite slightly higher ohmic and charge transfer resistance, and increased cell performance at high

current densities.

Graphene foam has advantages as alternative of flow field, which enhanced mass transport of reactants and water. Firstly, foam structure can improve reactants transport into catalyst layer. Figure 3.6 shows schematic representation of reactant pathway in flow field of compressed graphene foam MEA and conventional MEA. Considering in the in-plane direction, reactant flow just passes through flow field in conventional MEA. On the other hand, compressed graphene foam makes tortuous pathway of reactants thereby increasing retention time of reactants and diffusing more reactants into GDL. In through-plane direction, high porosity of graphene foam distributes reactant throughout an entire area of catalyst layer. While the area ratio between channel and rib of conventional flow field is 1:1, graphene foam has large channel area and directly transports more reactant into GDL based on diffusion plus convection [21]. Also Kuran et al [35] applied two-dimensional cross-the-channel model and demonstrated high channel-rib ratio of flow field improved performance due to enhanced reactant transport.

Additionally, compressed graphene foam can remove efficiently generated water. Hydrophobicity of flow field influences water removal. To examine hydrophobicity of graphene foam and conventional flow field, we conducted contact angle analyzer. Figure 3.7 shows that the contact angles of graphene foam and conventional flow field. The contact angle of graphene foam

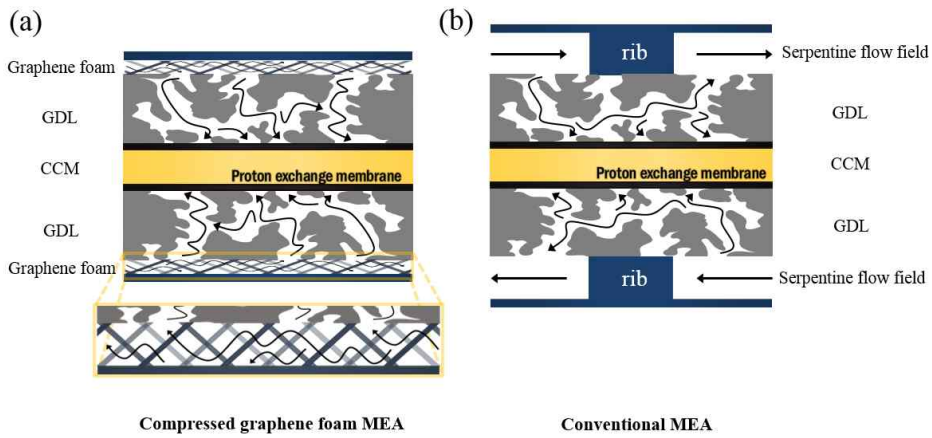

Figure 3.6 Schematic representation of reactant flow in flow field of (a) compressed graphene foam MEA and (b) conventional MEA.

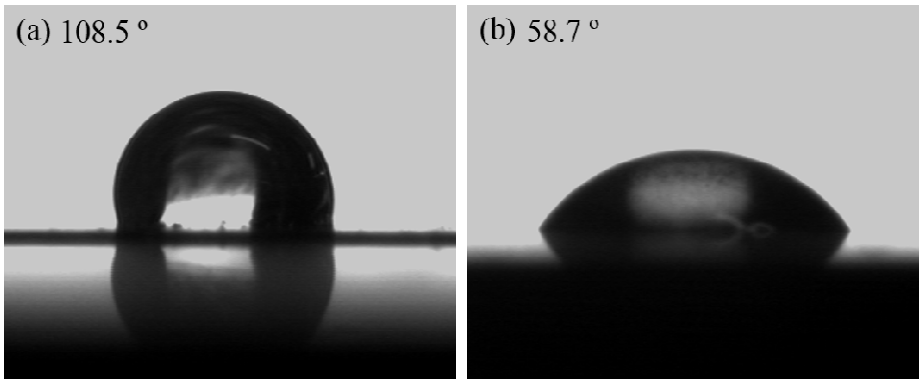

Figure 3.7 Contact angles of water droplets on (a) graphene foam and (b) conventional flow field

108.5 °. This result means graphene foam is hydrophobic. However, contact angle of conventional flow field is 58.7 °, which means it is hydrophilic. Therefore, unlike hydrophilic flow field, graphene foam is hydrophobic. Hydrophobic flow field is easier to remove generated water than hydrophilic flow field by inhibiting water flooding. Turhan et al characterized through-plane water behavior in hydrophobic channel wall using PTFE treatment. They asserted that liquid film was formed in hydrophilic flow field. In other hand, PTFE-treated flow field, which was hydrophobic, made water droplet on channel wall, which was easier to purge generated water droplets [32]. Also, water on hydrophilic substrate had more surface binding than on hydrophobic surface. So water on hydrophobic surfaces was found to be diffusive [33]. As graphene foam is hydrophobic, it can form water droplet, not water film. Additionally, while Tzseng et al [18] treated nickel foam with PTFE to increase hydrophobicity, we used graphene foam without PTFE treatment as flow field due to hydrophobicity of graphene foam.

In addition to forming water droplet on graphene foam, decreased thickness of graphene foam by compression is beneficial to water removal. Thickness of conventional flow field is 1 mm. However, we used compressed graphene foam to diffuse more reactants into GDL and increase conductivity of graphene foam. Reducing thickness from 1 mm to 150 μm induced faster flow velocity due to decreased volume of flow field. Faster

flow velocity is easier to pull water droplet in flow field. As a result, generated water can form water droplet due to hydrophobicity of graphene foam, and faster velocity accelerated by decreased thickness of graphene foam can drive excess water droplet along reactant flow, as shown in Figure 3.8. Therefore, graphene foam enabled to distribute uniformly reactants on entire area and remove efficiently generated water by eliminating water flooding.

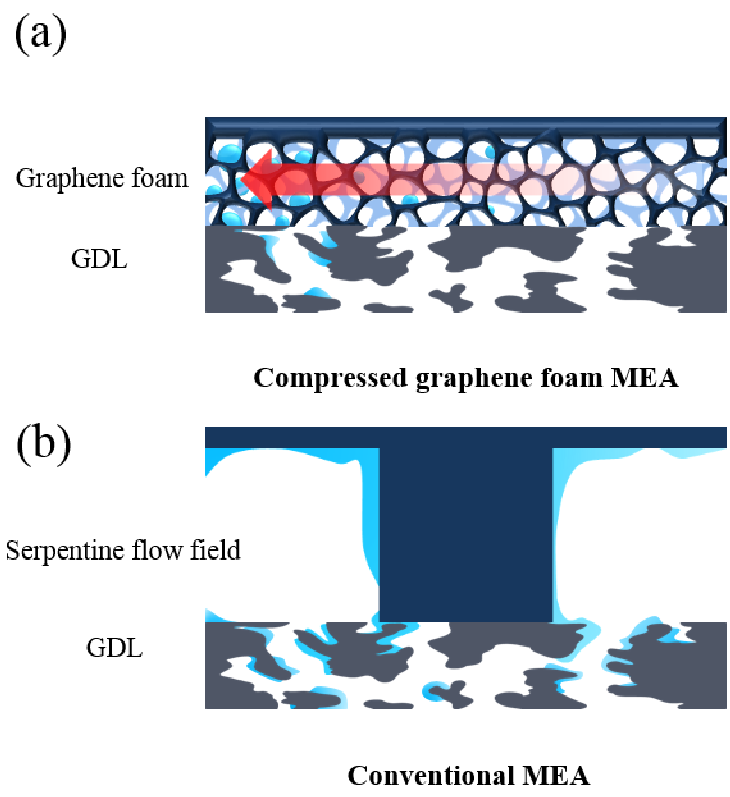

Figure 3.8 Schematic representations of water removal of (a) compressed graphene foam MEA and (b) conventional MEA

3.2 Application of graphene foam using as combined component of GDL and flow field on GDL-less MEA in fuel cells

Gas diffusion layer (GDL) is porous carbon material made by pressing carbon fibers into a carbon paper. It diffuses reactants from channel of bipolar plates to catalyst layer in through-plane direction and removes generated water outside of catalyst layer. Additionally, it connects electron transport between bipolar plates and catalyst layer, and provides mechanical support to MEA [1]. GDL is important component for water management in PEMFCs. Conventional GDL consists of polytetrafluoroethylene (PTFE)-treated carbon paper and micro-porous layer (MPL). PTFE coating, which is hydrophobic treatment, helps remove water from catalyst layer and prevent water flooding. MPL acts as smooth layer that provides large surface area for catalyst and good contact between porous carbon paper and catalyst layer.

Although GDL has high electrical conductivity, GDL causes electrical resistance and mass transport resistance. Also, GDLs occupy large volume in MEA because two GDLs (500 μm thick) is much thicker than CCM (~ 70 μm thick). Eliminating GDLs from MEA can reduce electrical resistance due to reduction of components, and decrease mass transport resistance because reactant pathway from bipolar plates to catalyst layer is decreased.

Additionally, lower thickness of MEA of single cell can lead to decreased volume of stack and increased volume power density. GDL-less MEA enhanced performance of single cell as well as volume power density of stacks.

To eliminate GDL from MEA, alternative which functions as GDL and flow field is needed. As shown in Figure 3.9 (a), we applied GDL on combined component of GDL and flow field by eliminating flow field in bipolar plate (Conventional MEA without flow field). Figure 3.9 (b) shows the polarization curves of conventional MEAs with and without flow field. The test was conducted using fully humidified H_2/O_2. Conventional MEA without flow field dropped below 0.7 $A \cdot cm^{-2}$ unlike conventional MEA with flow field. This result is due to insufficient supply of reactants. GDL is material fabricated by pressing carbon nanofiber into carbon paper, which has through-plane pores, not in-plane pores. So GDL did not function as flow field and is inappropriate alternative for combined component of GDL and flow field.

On the other hand, graphene foam is porous material, and also has in-plane and through-plane pores. Compressed graphene foam retains in-plane pores and can play a role in flow field. Also, high porosity in through-plane direction and hydrophobicity of graphene foam can function as GDL without any additional treatment. As discussed in previous work, graphene foam

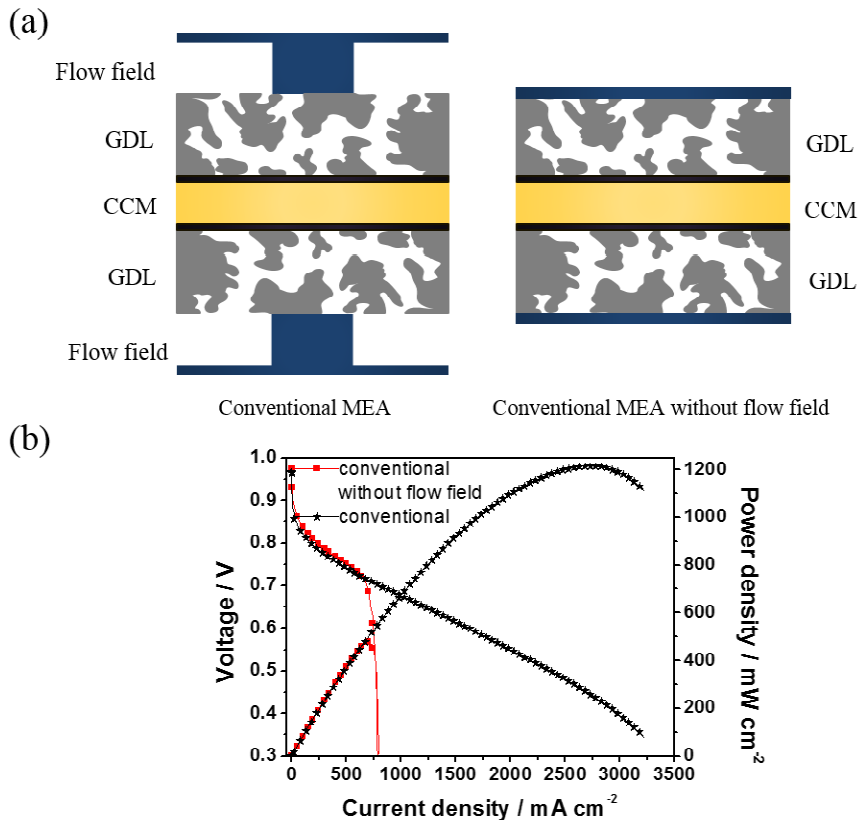

Figure 3.9 (a) Schematic of MEAs with flow field and without flow field. (b) Polarization curve of MEAs with flow field and without flow field.

Test at 70 °C H_2/O_2, fully humidified with ambient pressure.

must be compressed to achieve enhanced performance of single cell. The thickness and porosity of pristine graphene foam is 1 mm and 96.25 %, respectively. High porosity > 90 % causes reactants not to diffuse into GDL but to pass through flow field. So graphene foam must be compressed to achieve high performance. As thickness of graphene foam decreases, performance of graphene foam MEA can be enhanced because compressed graphene foam increases electrical conductivity and makes tortuous reactant pathway, which results in diffusion of more reactants into GDL. However, too thin graphene foam can block in-plane pores and then supply insufficient reactant to catalyst layer. Therefore, the thickness of graphene foam needs to be optimized to achieve high performance.

To investigate the optimal thickness of graphene foam, five different graphene foams were tested having different thicknesses; 1mm, 250 μm, 200 μm, 150 μm, and 100 μm. SEM images of graphene foams are shown in Figure 3.10. Figure 3.10 (a) and (b) show the top view and the cross-section of pristine graphene foam. After compression, all graphene foams have similar top views, as shown in Figure 3.10 (a). Figure 3.10 (c)-(f) represent the cross-section of graphene foams (250, 200, 150, and 100 μm). Graphene foam compressed from 1 mm to 250 μm formed layer-by-layer morphology and had the largest in-plane pores among 250, 200, 150, and 100 μm. Graphene foam which had thicknesses of 150 μm and 200 μm had similar

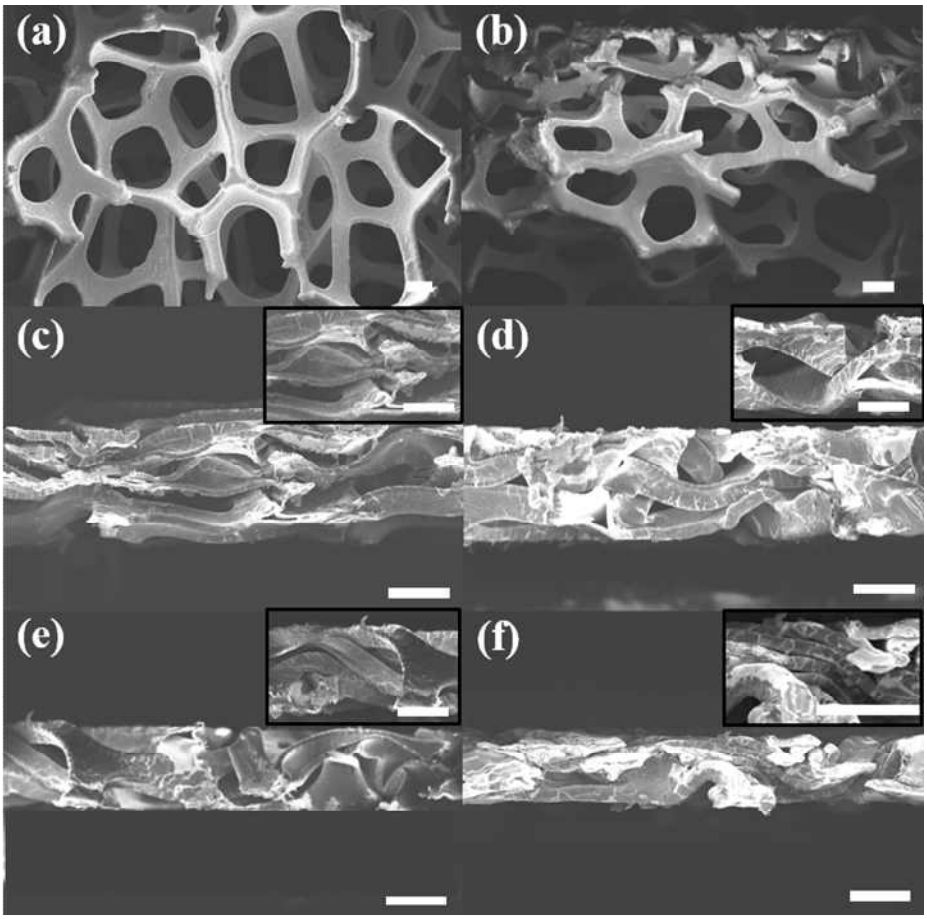

Figure 3.10 SEM images of graphene foams (a) top view of pristine graphene foam, and cross-sectional view of (b) pristine graphene foam, (c) 250 μm, (d) 200 μm, (e) 150 μm, and (f) 100 μm.

morphology of cross-section, as shown in Figure 3.10 (d) and (e), and graphene foam (200 μm) had larger in-plane pores than graphene foam (150 μm). Unlike three graphene foams, compression from 1 mm to 100 μm caused to block in-plane pores due to too thin thickness.

Figure 3.11 shows the single cell performance of five graphene foam MEAs. All fuel cell components and operating condition of graphene foam MEAs were held constant, except for the thickness of graphene foam. At low current densities that is dominant on activation loss, decreasing the thickness of graphene foam led to increasing performance of single cell. Generally, the activation loss for each GF MEA must be same because CCMs and graphene foam have similar properties [14, 32]. However, Figure 3.11 represents decreased thickness of graphene foam resulted in decreased activation loss. Activation loss is associated with exchange current density. Increased exchange current density represents decreased activation loss. Exchange current density is related to temperature, activation barrier, and reactant concentration. To decrease activation loss by increasing exchange current density, it is needed to increase temperature, use effective catalyst, or increase reactant concentration with higher outlet pressure [2]. Among these factors, decreased activation loss of GF MEAs can be affected by increased reactant concentration with higher outlet pressure because we used same CCM and operated in same condition. Therefore, reduced thickness of

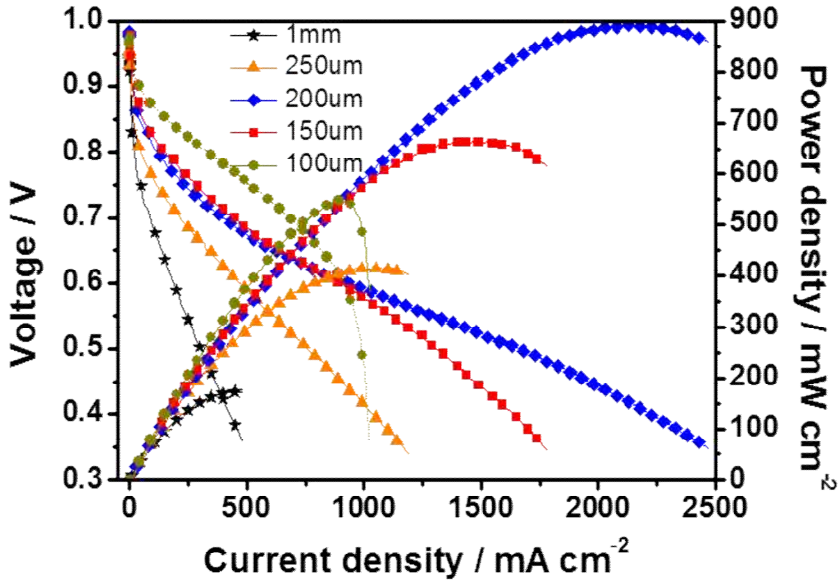

Figure 3.11 Polarization curves of MEAs with varying graphene foam thickness

graphene foam increased internal pressure in graphene foam. When supplying certain flow rate of reactants, decreased volume in graphene foam resulted in higher pressure, thereby decreasing activation loss. Therefore, decreased thickness of graphene foam increased performance by reducing activation loss in low current densities.

However, five MEAs did not show same tendency in high current densities. Compression from 1 mm to 200 μm increased performance in overall current densities due to increased pressure. However, graphene foams that had thicknesses of less than 200 μm reduced in-pore sizes and declined mass transport, leading to decreased performance in high current densities. Furthermore, 100 μm-GF MEA dropped below 1 $A \cdot cm^{-2}$ despite high voltage at low current densities. This result is consistent with conventional MEA without flow field. It indicated that decreasing the thickness of graphene foam from 1 mm to 100 μm caused the blocking of in-plane pores, resulting in insufficient in-plane supply of reactants, as shown in Figure 3.10 (f). As a result, 200 μm is optimal thickness that exhibited the highest performance.

Figure 3.12 and Table 3.3 represents comparison between 200 μm-GF MEA and conventional MEA. 200 μm-GF MEA exhibited higher voltage than conventional in overall current densities. Especially, 200 μm-GF MEA resulted in an increase by 56% and 74% at 0.4 V and 0.8 V, respectively.

Current density at 0.8 V was 120mA·cm^{-2}, which is 74% higher than conventional MEA (69 mA·cm^{-2}). This result indicates the 200 μm-GF MEA reduced activation loss due to increased internal pressure by reducing volume flowing reactants. This effect is similar with the effect of outlet pressure. In other words, 200 μm-GF MEA decreased activation loss without outlet pressure. In low cell voltage (0.4 V), which is dominant on mass transport, 200 μm-GF MEA performed larger current density than conventional MEA. It is attributed to substituting graphene foam with GDL and flow field. Eliminating GDL from MEA and decreased thickness of graphene foam reduced reactant pathway by about 84%, resulting in reduced mass transport resistance. It is consistent with application of graphene foam on flow field. Also, increased internal pressure pulled water droplet easily by inhibiting water flooding. In 0.6 V, current density of 200 μm-GF MEA was higher than conventional MEA although graphene foam MEA did not have micro-porous layer (MPL). Conventional MEA has GDLs which include MPL. MPL provides surface area and good contact with entire area of catalyst layer. In the other hand, 200 μm-GF MEA did not have MPL, so electron transport was lower than conventional MEA, which affected middle current densities. However, current density of 200 μm-GF MEA at0.6 V increased by 16% due to upshift of performance by increased internal pressure. As a result, power density of 200 μm GF-MEA was increased by

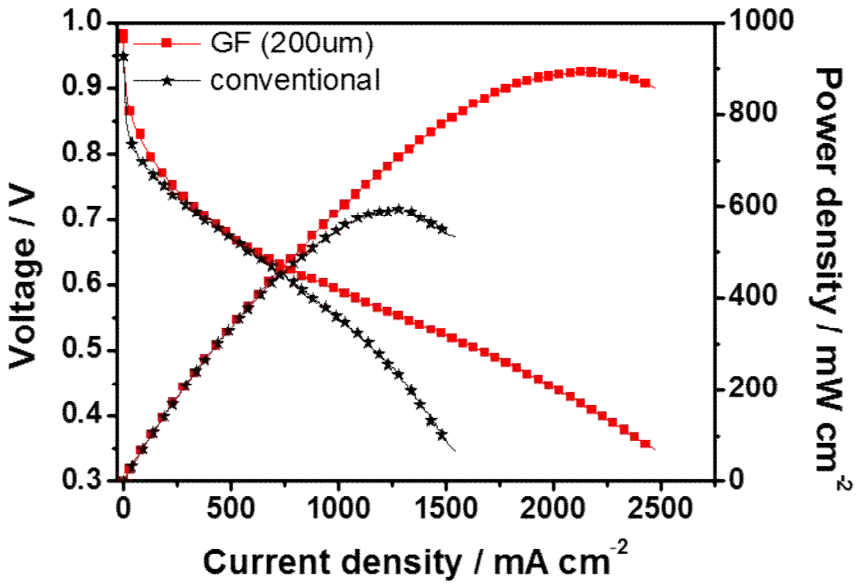

Figure 3.12 Polarization curves 200 μm-GF MEA and conventional MEA with ambient pressure. For both MEAs, the catalyst loading was 0.2 $mg \cdot cm^{-2}$. Test at 70 °C H_2/air with ambient pressure.

Table 3.3. Comparison in current density of 200 μm-GF MEA and conventional MEA (mA·cm^{-2})

	0.8V	0.6V	0.4V
200 μm-GF MEA	120 (174%)	939 (116%)	2218 (156%)
Conventional MEA	69	809	1419

50% and thickness of MEA was decreased by 85%. Therefore, volume power density can be maximized by 210%.

To examine the mass transport phenomena of graphene foam MEA, oxygen gain and electrochemical impedance spectroscopy (EIS) were conducted. Oxygen gain is difference between cell voltage under oxygen and air condition. While cell voltage under oxygen condition excludes mass transport effect, cell voltage under air condition is affected by mass transport resistance due to decreased oxygen partial pressure and blanketing effect of nitrogen [37]. Therefore, mass transport resistance can be measured by the oxygen gain. In other words, lower oxygen gain means reduced mass transport resistance, leading to enhanced mass transport of reactant and product. Figure 3.13 shows the oxygen gain of 200 μm-GF MEA and conventional MEA. In high current densities, the oxygen gain of 200 μm-GF MEA was much lower than that of conventional MEA. This result indicates the design by using graphene foam as GDL and flow field reduced mass transport resistance.

Electrochemical impedance spectroscopy (EIS) is diagnostic tool used to measure the frequency-dependent impedance of fuel cell by applying AC potential as perturbation signal and measuring the current [42]. This tool has advantage of analyzing individual contributions such as ohmic, charge transfer, and mass transport resistance in total impedance. Modified Randles

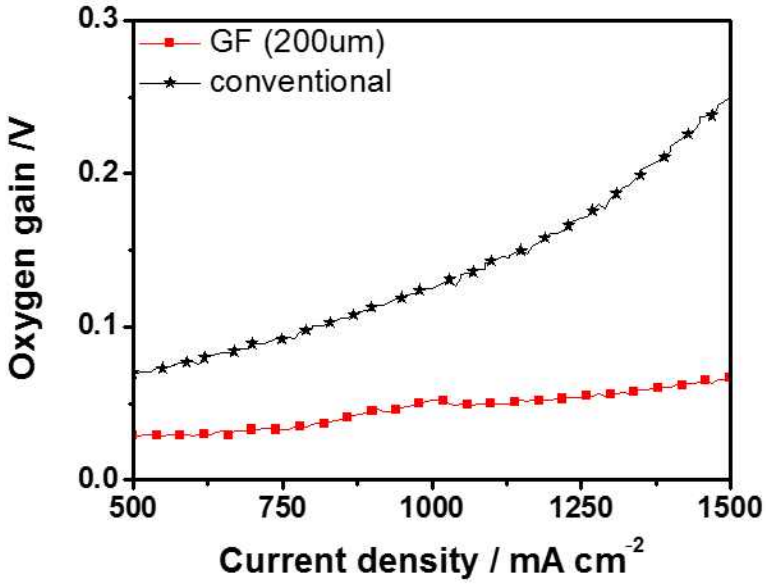

Figure 3.13 Oxygen gain graph with 200 μm-GF MEA and conventional MEA in high current densities.

model was chosen in this study as shown in Figure 3. 14 (a). Figure 3.14 (b) and (c) are Nyquist plot, which is the plot of imaginary part of impedance versus the real part at each frequency. Ohmic resistance, $R_{\Omega,}$ is the sum of ionic and electronic resistances of cell components. Charge transfer resistance, $R_{ct,}$ is related to activation losses, which is function of catalyst surface area, catalyst concentration, and catalyst utilization [2, 43]. Warburg impedance, Zw, is related to mass transport resistance. In Nyquist plot, high frequency intercept is ohmic resistance and diameter of semicircle represents charge transfer resistance in high cell voltage (0.8 V). However, in low cell voltage (0.4 V), which is dominant region of mass transport polarization, the semicircle of Nyquist plot indicates both charge transfer and mass transfer resistances [44]. High-frequency semicircle means charge transfer resistance and low-frequency semicircle indicates mass transfer resistance.

Figure 3. 14 (b) represents the Nyquist plot at 0.4 V of 200 μm-GF MEA and conventional MEA. Ohmic resistance of 200 μm-GF MEA was larger than that of conventional MEA. This result is consistent with [17, 32] because electron pathway of conventional MEA is vertical but graphene foam MEA conducts electron vertically and horizontally. Also graphene foam MEA did not include MPL, so contact area between graphene foam and catalyst layer was decreased, leading to reduced electronic conductivity and increased ohmic resistance. Although 200 μm-GF MEA had larger

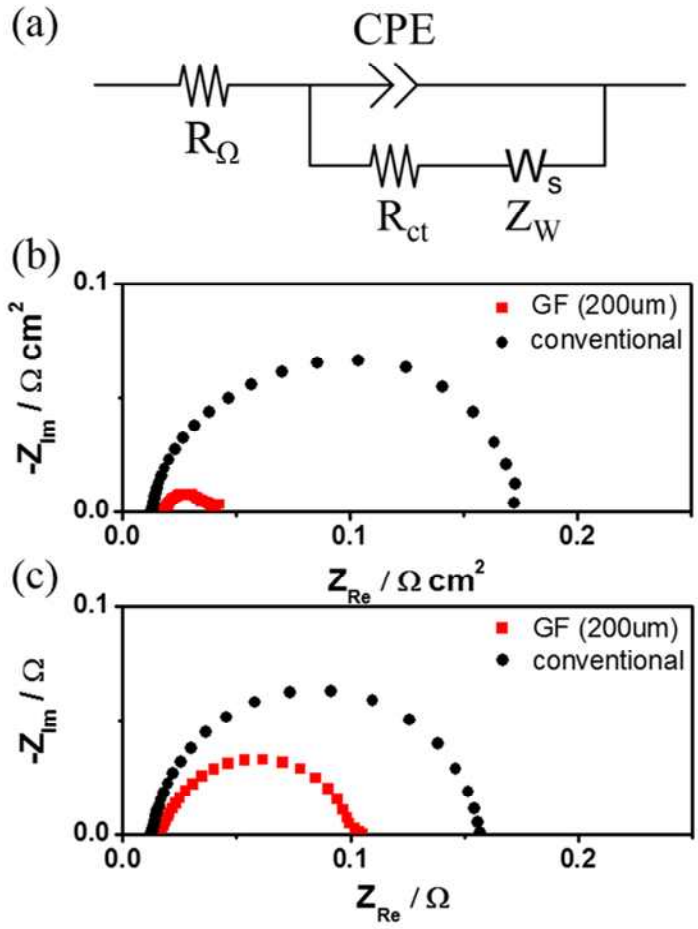

Figure 3.14 Electrochemical impedance spectroscopy (a) Randles equivalent circuit model for EIS. EIS Nyquist plots of 200 μm-GF MEA and conventional MEA at (b) 0.4 and (c) 0.8 V under a fully humidified H_2/air.

ohmic resistance, mass transfer resistance of 200 μm-GF MEA was much smaller than that of conventional MEA. This result indicates that GDL-less MEA by using graphene foam decreased mass transport resistance and enhanced mass transport, leading to increased cell performance in high current densities.

Figure 3. 14 (c) shows the Nyquist plot at 0.8 V of 200 μm-GF MEA and conventional MEA. High cell voltage (0.8 V) is region which is dominant on activation polarization, so mass transport resistance can be neglected [45]. Although 200 μm-GF MEA had larger ohmic resistance, charge transfer resistance of 200 μm-GF MEA was smaller than that of conventional MEA. It is consistent result with polarization curve at low current densities. Cell polarization curve and EIS indicates the activation loss was decreased due to using graphene foam as GDL and flow field. As all fuel cell components and operating condition of graphene foam MEAs were held constant except for the thickness of graphene foam, activation loss of graphene foam MEA can be affected by increased reactant concentration by outlet pressure. However, as graphene foam MEA was performed at ambient pressure, activation loss was affected by internal pressure of graphene foam. Compressed graphene foam reduced pore size and changed internal pore structure, as shown in Figure 3.10. Compression of graphene foam and eliminating GDL reduced volume of flowing reactants and increased internal pressure. Increased

internal pressure in graphene foam was affected directly on catalyst layer because eliminating GDL induced direct contact between graphene foam and catalyst layer. Without outlet pressure, performance of 200 μm-GF MEA in low current densities was enhanced by reducing activation loss due to pressure formed inside graphene foam.

To examine the effect of eliminating GDL on cell performance, comparison of performance between 200 μm-GF MEA and 200 μm-GF MEA with GDL were conducted. Figure 3.15 (a) shows the schematic of 200 μm-GF MEA and 200 μm-GF MEA with GDL. Except GDL, all cell components and thickness of graphene foam were same. Figure 3.15 (b) represents the polarization curves of 200 μm-GF MEA and 200 μm-GF MEA with GDL. 200 μm-GF MEA outperformed 200 μm-GF MEA with GDL in overall current densities. It is attributed to lower ohmic loss of 200 μm-GF MEA due to elimination of GDL. Figure 3. 16 also shows that ohmic resistance of 200 μm-GF MEA was much lower than that of 200 μm-GF MEA with GDL. Ohmic resistance of 200 μm-GF MEA and 200 μm-GF MEA with GDL was 0.0152 Ω and 0.026 Ω, respectively. As ohmic loss of 200 μm-GF MEA was decreased by 42% compared to 200 μm-GF MEA with GDL, cell performance was enhanced. Also, IR-corrected cell voltage was conducted to investigate the effect of elimination GDL on activation and mass transport losses. IR-corrected cell voltage is identification of activation

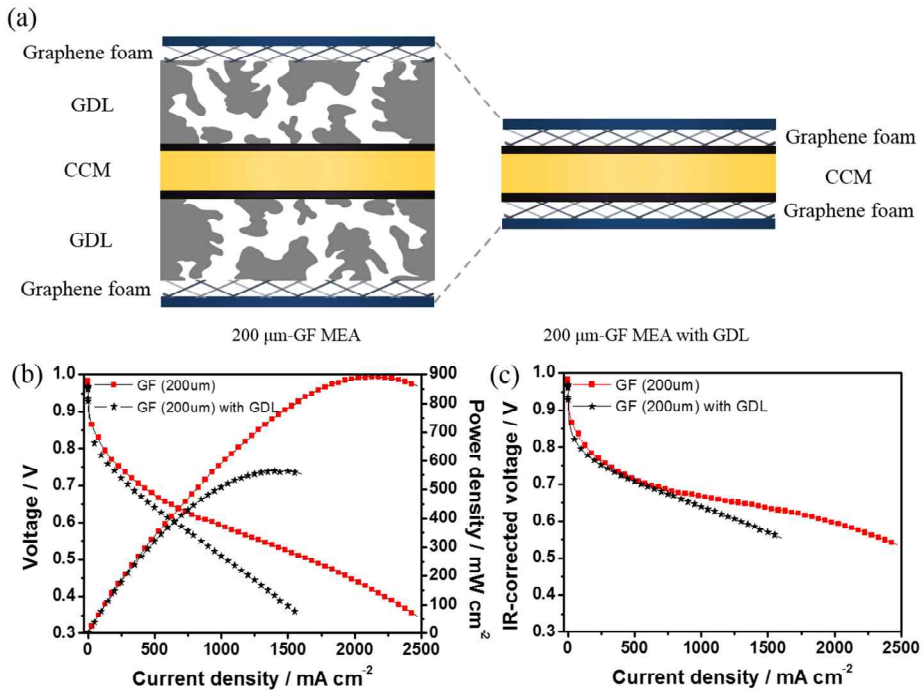

Figure 3.15 (a) Schematic of 200 μm-GF MEA and 200 μm-GF MEA with GDL. (b) Polarization curve of 200 μm-GF MEA and 200 μm-GF MEA with GDL. (c) IR-corrected voltage of 200 μm-GF MEA and 200 μm-GF MEA with GDL. Test at 70 °C H_2/air, fully humidified with ambient pressure.

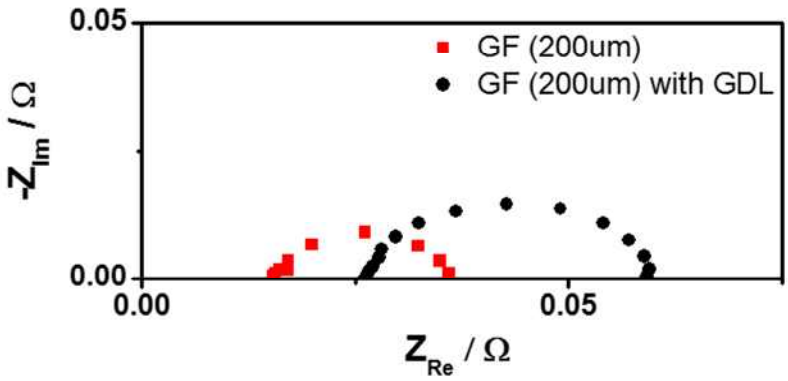

Figure 3.16 Electrochemical impedance spectroscopy of 200 µm-GF MEA and 200 µm-GF MEA with GDL at 0.6 V

and mass transport losses by eliminating ohmic effect of performance. It is useful tool for comparison of activation and mass transport effect between two MEAs [46]

$$V_{corr} = V_{cell} + \eta_{ohmic} \quad [29]$$

Figure 3.15 (c) represents the IR-corrected cell voltage of 200 μm-GF MEA and 200 μm-GF MEA with GDL. By eliminating ohmic loss, cell voltage was same in middle current densities. For 200 μm-GF MEA, internal pressure in graphene foam was increased and affected the cell voltage. However, internal pressure of 200 μm-GF MEA with GDL is much lower than 200 μm-GF MEA as thickness of 200 μm-GF MEA with GDL was 450 μm (Graphene foam: 200 μm and GDL: 250 μm). Therefore, 200 μm-GF MEA with GDL was not affected by internal pressure due to larger volume of flowing reactants. In high cell voltage, current density of 200 μm-GF MEA is larger than that of 200 μm-GF MEA with GDL due to increased internal pressure of 200 μm-GF MEA. Also, in low cell voltage, 200 μm-GF MEA exhibited higher current density. By reducing volume of flowing reactants due to elimination of GDL, increased internal pressure pulled generated water droplet easily. Therefore, 200 μm-GF MEA increased internal pressure in graphene foam, and enhanced activation and mass

transport overpotentials, leading to increased cell performance in overall current densities.

Chapter 4. Conclusions

In this thesis, flow-field/electrode unified MEA were applied on PEMFC to enhance performance by using graphene foam without any treatment and MPL. Graphene foam is three-dimensional material which has interconnected in-plane and through-plane pores. Firstly, single cell test of graphene foam as flow field was conducted. To investigate the effect of graphene foam as flow field on mass transport, graphene foam must be compressed to increase conductivity of graphene foam and diffuse more reactants into GDL. Compressed graphene foam as flow field provided smaller in-plane pores and made more tortuous pathway of reactants, leading to more reactants diffused into GDL. Also, large through-plane pores transported reactants on entire area of catalyst layer. Additionally, unlike conventional MEA, decreased flow field width by compression induced faster flow velocity and dragged water droplets through unused reactant flow. Therefore, improved mass transport of reactants and product increased performance of single cell by 30% at high current densities region. Also, oxygen gain and EIS were performed, representing that graphene foam as flow field influenced decreased mass transport resistance and increased cell performance.

Secondly, graphene foam was applied on GDL-less MEA without any

treatment and MPL. The thickness of graphene foam was optimized to achieve high performance. Decreasing the thickness of graphene foam resulted in higher performance at low current densities because increased internal pressure caused by decreased volume of graphene foam affected activation loss. However, too thin thickness blocked in-plane pores and declined mass transport. Therefore, 200 μm is optimal thickness of trade-off between internal pressure and mass transport. Performance of 200 μm GF-MEA increased in overall current densities. Increased internal pressure in graphene foam affected activation loss and increased performance in low current densities without outlet pressure. Also eliminating GDL reduced thickness of MEA and reactant pathway, leading to decreased mass transport resistance. Additionally, increased internal pressure helped remove water easily. Therefore, power density of 200 μm GF-MEA was increased by 50% and thickness of MEA was decreased by 85%. Also, volume power density can be maximized by 210%.

References

[1] Y. Wang, K. S. Chen, J. Mishler, S. C. Cho, X. C. Adroher, A review of polymer electrolyte membrane fuel cells: Technology, applications, and needs on fundamental research, Applied Energy, 88 (2011) 981-1007.

[2] Ryan P. O'Hayre, Suk-won Cha, Whitney G. Colella, F. B. Prinz, Fuel Cell Fundamentals, Wiley, New York, 2008.

[3] D. Garraín, Y. Lechón, C. d. l. Rúa, Polymer Electrolyte Membrane Fuel Cells (PEMFC) in Automotive Applications: Environmental Relevance of the Manufacturing Stage, Smart Grid and Renewable Energy, 02 (2011) 68-74.

[4] A. A. Kornyshev, A. M. Kuznetsov, E. Spohr, J. Ulstrup, Kinetics of Proton Transport in Water, The Journal of Physical Chemistry B, 107 (2003) 3351-3366.

[5] P. Y. Chen, C. P. Chiu, C. W. Hong, Molecular structure and transport dynamics in Nafion and sulfonated poly(ether ether ketone ketone) membranes, J. Power Sources, 194 (2009) 746-752.

[6] Y. Xiao, M. Dou, J. Yuan, M. Hou, W. Song, B. Sunden, Fabrication Process Simulation of a PEM Fuel Cell Catalyst Layer and Its Microscopic Structure Characteristics, J. Electrochem. Soc., 159 (2012) B308-B314.

[7] S. Litster, G. McLean, PEM fuel cell electrodes, J. Power Sources, 130

(2004) 61-76.

[8] H. Li, Y. Tang, Z. Wang, Z. Shi, S. Wu, D. Song, J. Zhang, K. Fatih, J. Zhang, H. Wang, Z. Liu, R. Abouatallah, A. Mazza, A review of water flooding issues in the proton exchange membrane fuel cell, J. Power Sources, 178 (2008) 103-117.

[9] F.-Y. Zhang, S. G. Advani, A. K. Prasad, Performance of a metallic gas diffusion layer for PEM fuel cells, J. Power Sources, 176 (2008) 293-298.

[10] H. Choi, O. H. Kim, M. Kim, H. Choe, Y. H. Cho, Y. E. Sung, Next-generation polymer-electrolyte-membrane fuel cells using titanium foam as gas diffusion layer, ACS applied materials & interfaces, 6 (2014) 7665-7671.

[11] X. Li, I. Sabir, Review of bipolar plates in PEM fuel cells: Flow-field designs, Int. J. Hydrogen Energy, 30 (2005) 359-371.

[12] D. H. Jeon, S. Greenway, S. Shimpalee, J. W. Van Zee, The effect of serpentine flow-field designs on PEM fuel cell performance, Int. J. Hydrogen Energy, 33 (2008) 1052-1066.

[13] A. Turhan, K. Heller, J. S. Brenizer, M. M. Mench, Passive control of liquid water storage and distribution in a PEFC through flow-field design, J. Power Sources, 180 (2008) 773-783.

[14] A. K. Srouji, L. J. Zheng, R. Dross, A. Turhan, M. M. Mench, Performance and mass transport in open metallic element architecture fuel cells at ultra-high current density, J. Power Sources, 218 (2012) 341-347.

[15] A. K. Srouji, L. J. Zheng, R. Dross, A. Turhan, M. M. Mench, Ultra-high current density water management in polymer electrolyte fuel cell with porous metallic flow field, J. Power Sources, 239 (2013) 433-442.

[16] T. Kariya, T. Hirono, H. Funakubo, T. Shudo, Effects of the porous structures in the porous flow field type separators on fuel cell performances, Int. J. Hydrogen Energy, 39 (2014) 15072-15080.

[17] S. Tanaka, T. Shudo, Significant performance improvement in terms of reduced cathode flooding in polymer electrolyte fuel cell using a stainless-steel microcoil gas flow field, J. Power Sources, 248 (2014) 524-532.

[18] A. Kumar, R. G. Reddy, Materials and design development for bipolar/end plates in fuel cells, J. Power Sources, 129 (2004) 62-67.

[19] Y. Wang, Porous-Media Flow Fields for Polymer Electrolyte Fuel Cells, J. Electrochem. Soc., 156 (2009) B1124.

[20] B.-T. Tsai, C.-J. Tseng, Z.-S. Liu, C.-H. Wang, C.-I. Lee, C.-C. Yang, S.-K. Lo, Effects of flow field design on the performance of a PEM fuel cell with metal foam as the flow distributor, Int. J. Hydrogen Energy, 37 (2012) 13060-13066.

[21] C.-J. Tseng, B. T. Tsai, Z.-S. Liu, T.-C. Cheng, W.-C. Chang, S.-K. Lo, A PEM fuel cell with metal foam as flow distributor, Energy Convers. Manage., 62 (2012) 14-21.

[22] T.-Y. Jeon, S. J. Yoo, Y.-H. Cho, K.-S. Lee, S. H. Kang, Y.-E. Sung,

Influence of Oxide on the Oxygen Reduction Reaction of Carbon-Supported Pt−Ni Alloy Nanoparticles, The Journal of Physical Chemistry C, 113 (2009) 19732-19739.

[23] C. Zhang, S. Y. Hwang, A. Trout, Z. Peng, Solid-State Chemistry-Enabled Scalable Production of Octahedral Pt–Ni Alloy Electrocatalyst for Oxygen Reduction Reaction, J. Am. Chem. Soc., 136 (2014) 7805-7808.

[24] D. Wang, H. L. Xin, R. Hovden, H. Wang, Y. Yu, D. A. Muller, F. J. DiSalvo, H. D. Abruña, Structurally ordered intermetallic platinum–cobalt core–shell nanoparticles with enhanced activity and stability as oxygen reduction electrocatalysts, Nat Mater, 12 (2013) 81-87.

[25] X. Zhou, Y. Gan, J. Du, D. Tian, R. Zhang, C. Yang, Z. Dai, A review of hollow Pt-based nanocatalysts applied in proton exchange membrane fuel cells, J. Power Sources, 232 (2013) 310-322.

[26] O. H. Kim, Y. H. Cho, S. H. Kang, H. Y. Park, M. Kim, J. W. Lim, D. Y. Chung, M. J. Lee, H. Choe, Y. E. Sung, Ordered macroporous platinum electrode and enhanced mass transfer in fuel cells using inverse opal structure, Nat Commun, 4 (2013) 2473.

[27] X. Dominguez-Benetton, S. Sevda, K. Vanbroekhoven, D. Pant, The accurate use of impedance analysis for the study of microbial electrochemical systems, Chem. Soc. Rev., 41 (2012) 7228-7246.

[28] S. Haji, Analytical modeling of PEM fuel cell i–V curve, Renewable

Energy, 36 (2011) 451-458.

[29] M. V. Williams, H. R. Kunz, J. M. Fenton, Analysis of polarization curves to evaluate polarization sources in hydrogen/air PEM fuel cells, J. Electrochem. Soc., 152 (2005) A635-A644.

[30] J. Benziger, E. Kimball, R. Mejia-Ariza, I. Kevrekidis, Oxygen mass transport limitations at the cathode of polymer electrolyte membrane fuel cells, AlChE J., 57 (2011) 2505-2517.

[31] Z. Chen, W. Ren, L. Gao, B. Liu, S. Pei, H. M. Cheng, Three-dimensional flexible and conductive interconnected graphene networks grown by chemical vapour deposition, Nature Materials, 10 (2011) 424-428.

[32] S. Tanaka, T. Shudo, Corrugated mesh flow channel and novel microporous layers for reducing flooding and resistance in gas diffusion layer-less polymer electrolyte fuel cells, J. Power Sources, 268 (2014) 183-193.

[33] Y.-H. Cho, J. W. Lim, Y. S. Kang, Y.-H. Cho, O.-H. Kim, N.-H. Kwon, O. J. Kwon, W.-S. Yoon, H. Choe, Y.-E. Sung, The dependence of performance degradation of membrane electrode assembly on platinum loading in polymer electrolyte membrane fuel cell, Int. J. Hydrogen Energy, 37 (2012) 2490-2497.

[34] M. Ahn, Y.-H. Cho, Y.-H. Cho, J. Kim, N. Jung, Y.-E. Sung, Influence of hydrophilicity in micro-porous layer for polymer electrolyte membrane

fuel cells, Electrochim. Acta, 56 (2011) 2450-2457.

[35] W. Sun, B. A. Peppley, K. Karan, Modeling the Influence of GDL and flow-field plate parameters on the reaction distribution in the PEMFC cathode catalyst layer, J. Power Sources, 144 (2005) 42-53.

[36] J. Lee, J. M. Yoo, Y. Ye, Y. Mun, S. Lee, O. H. Kim, H. W. P. Rhee, H. I. D. Lee, Y. E. Sung, J. P. Lee, Development of highly stable and mass transfer-enhanced cathode catalysts: Support-free electrospun intermetallic FePt nanotubes for polymer electrolyte membrane fuel cells, Advanced Energy Materials, 5 (2015).

[37] M. Prasanna, H. Y. Ha, E. A. Cho, S. A. Hong, I. H. Oh, Investigation of oxygen gain in polymer electrolyte membrane fuel cells, J. Power Sources, 137 (2004) 1-8.

[38] F. Liu, B. Yi, D. Xing, J. Yu, Z. Hou, Y. Fu, Development of novel self-humidifying composite membranes for fuel cells, J. Power Sources, 124 (2003) 81-89.

[39] Z. Xie, S. Holdcroft, Polarization-dependent mass transport parameters for orr in perfluorosulfonic acid ionomer membranes: An EIS study using microelectrodes, J. Electroanal. Chem., 568 (2004) 247-260.

[40] J. W. Lim, Y.-H. Cho, M. Ahn, D. Y. Chung, Y.-H. Cho, N. Jung, Y. S. Kang, O.-H. Kim, M. J. Lee, M. Kim, Y.-E. Sung, Ionic Resistance of a Cathode Catalyst Layer with Various Thicknesses by Electrochemical

Impedance Spectroscopy for PEMFC, J. Electrochem. Soc., 159 (2012) B378.

[41] J. S. Yi, T. w. Song, Performance Characterization of PEM Fuel Cells Using AC Impedance Spectroscopy: I. Model-Based Analysis, J. Electrochem. Soc., 160 (2012) F141-F152.

[42] X. Yuan, H. Wang, J. Colinsun, J. Zhang, AC impedance technique in PEM fuel cell diagnosis—A review, Int. J. Hydrogen Energy, 32 (2007) 4365-4380.

[43] S. Y. Cha, W. M. Lee, Performance of Proton Exchange Membrane Fuel Cell Electrodes Prepared by Direct Deposition of Ultrathin Platinum on the Membrane Surface, J. Electrochem. Soc., 146 (1999) 4055-4060.

[44] D. Malevich, E. Halliop, B. A. Peppley, J. G. Pharoah, K. Karan, Investigation of Charge-Transfer and Mass-Transport Resistances in PEMFCs with Microporous Layer Using Electrochemical Impedance Spectroscopy, J. Electrochem. Soc., 156 (2009) B216.

[45] Y. Tang, J. Zhang, C. Song, H. Liu, J. Zhang, H. Wang, S. Mackinnon, T. Peckham, J. Li, S. McDermid, P. Kozak, Temperature Dependent Performance and In Situ AC Impedance of High-Temperature PEM Fuel Cells Using the Nafion-112 Membrane, J. Electrochem. Soc., 153 (2006) A2036.

[46] M. S. Naughton, A. A. Moradia, P. J. A. Kenis, Quantitative Analysis of

Single-Electrode Plots to Understand In-Situ Behavior of Individual Electrodes, J. Electrochem. Soc., 159 (2012) B761.

국문초록

연료전지는 화학에너지를 전기화학 반응을 통해 전기에너지로 직접 변환시키는 에너지 변환 장치이다. 이러한 연료전지 중에 고분자 전해질 연료전지(PEMFC)는 낮은 작동온도와 높은 출력밀도, 빠른 시동의 이점으로 인해 운송이나 휴대용 전자기기 적용에는 적합한 반면 구성요소들의 가격부담과 현재 가장 많이 사용하고 있는 촉매인 백금의 매장량 부족 및 장기안정성 부족으로 아직 상용화는 되지 못하는 실정이다. 따라서 백금의 사용량을 줄이거나 백금기반촉매를 비 귀금속 촉매로 대체하는 방법을 통해 저렴하면서도 장기 안정성까지 갖춘 촉매 개발 연구들이 다양하게 시도되고 있다. 또한 기존의 백금촉매를 이용하면서 촉매 층이나 다른 구성요소들의 구조를 바꾸고 새롭게 디자인하여 단위전지의 성능을 증대시키는 연구도 많이 진행되어 오고 있다.

단위전지 구성요소들과 관련된 최근 연구들은 기존의 분리판(bipolar plate) 내부에 설계되어 있는 가스유로(flow field)를 금속 가루(powder)나 금속 코일(coil), 금속 망(mesh), 금속 폼(foam) 등과 같은 기공이 많은 물질들로 대체함으로써 물질전달을 개선한 연구결과들을 보고해왔다. 그리고 더 나아가 이러한 다공성물질들을 기체확산층(GDL)과 가스유로로 사용함으로써 기존 단위전지 구조를 기체확산층을 제거한 구조로 변화시키는 연구도 개발되었다.

이 기체확산층이 없는 구조는 반응물의 이동경로를 단축시킴으로써 물질전달 저항을 줄여주고 단위전지 성능을 증가시킨다는 이점을 가지고 있지만, 기존의 기체확산층의 구조 중 하나인 미세다공층(MPL)은 여전히 포함하고 있다.

본 연구의 목적은 그래핀 폼(graphene foam)을 구성요소로 사용하여 단위전지 성능을 증대시키는데 있다. 그래핀 폼은 금속 폼과 동일한 구조를 가지고 있지만 구성 물질이 다르기 때문에 기존의 금속 폼이 가지고 있는 부식이나 오염 문제를 해결할 수 있다. 즉, 그래핀 폼은 금속 폼이 가지는 구조적 이점을 유지하면서 금속의 단점을 없앤 물질이라 할 수 있다.

본 연구에서는 그래핀 폼을 기체확산층과 가스유로를 통합시킨 일체형 막-전극 접합체(MEA)를 제작하여 물질전달 저항을 줄이고 막-전극 접합체의 두께를 현저히 줄여 단위전지의 성능을 증가시켰을 뿐만 아니라 스택(stack)의 부피 출력 밀도도 극대화시켰다. 일체형 막-전극 접합체를 제작하기 위해서는 그래핀 폼이 가스유로와 기체확산층으로 사용되었을 때 성능에 끼치는 영향을 분석하고 최적화하는 단계가 필요하였다. 먼저, 그래핀 폼을 가스유로로 대체하여 단위전지 성능 테스트와 전기화학 분석을 연구한 결과, 그래핀 폼을 가스유로로 사용함으로써 반응물이 촉매층 전체에 고르게 분포되었고, 생성물인 물도 잘 배출되어 물질 전달을 개선시키는 것으로 나타났다.

두 번째, 그래핀 폼을 기체확산층이 없는 단위전지에 적용시켜 그래핀 폼이 가스유로의 역할뿐만 아니라 기체확산층의 역할을 할 수 있는지 성능 테스트를 하였다. 그 결과, 미세다공층이 존재하지 않고 어떠한 처리를 하지 않았음에도 불구하고, 출력 밀도가 50% 나 증가하였고, 동시에 막-전극 접합체의 두께도 90%나 감소하여, 부피 출력 밀도가 크게 향상되는 것을 확인하였다.

따라서 본 연구에서 제시한 일체형 막-전극 접합체 제작 방법과 주목할 만한 성능효과는 상용 연료전지에 적용할 수 있다는 가능성을 보여주었다.

핵심어 : 고분자 전해질 연료전지, 그래핀 폼, 가스유로, 기체확산층, 일체형 막-전극 접합체

학 번 : 2014-20628